



**HAL**  
open science

**Morphological characterization and thermal properties  
of compatibilized  
poly(3-hydroxybutyrate-co-3-hydroxyvalerate)  
(PHBV)/poly(butylene succinate) (PBS)/halloysite  
ternary nanocomposites**

Salima Kennouche, Nicolas Le Moigne, Mustapha Kaci, Jean-Christophe  
Quantin, Anne-Sophie Caro-Bretelle, Christelle Delaite, José-Marie  
Lopez-Cuesta

► **To cite this version:**

Salima Kennouche, Nicolas Le Moigne, Mustapha Kaci, Jean-Christophe Quantin, Anne-Sophie Caro-Bretelle, et al.. Morphological characterization and thermal properties of compatibilized poly(3-hydroxybutyrate-co-3-hydroxyvalerate) (PHBV)/poly(butylene succinate) (PBS)/halloysite ternary nanocomposites. *European Polymer Journal*, 2016, 75, pp.142-162. 10.1016/j.eurpolymj.2015.12.009 . hal-02906421

**HAL Id: hal-02906421**

**<https://hal.science/hal-02906421v1>**

Submitted on 25 Jan 2021

**HAL** is a multi-disciplinary open access archive for the deposit and dissemination of scientific research documents, whether they are published or not. The documents may come from teaching and research institutions in France or abroad, or from public or private research centers.

L'archive ouverte pluridisciplinaire **HAL**, est destinée au dépôt et à la diffusion de documents scientifiques de niveau recherche, publiés ou non, émanant des établissements d'enseignement et de recherche français ou étrangers, des laboratoires publics ou privés.

# Morphological characterization and thermal properties of compatibilized poly(3-hydroxybutyrate-co-3-hydroxyvalerate) (PHBV)/poly(butylene succinate) (PBS)/halloysite ternary nanocomposites

Salima Kennouche<sup>a,b</sup>, Nicolas Le Moigne<sup>b,\*</sup>, Mustapha Kaci<sup>a</sup>, Jean-Christophe Quantin<sup>b</sup>, Anne-Sophie Caro-Bretelle<sup>b</sup>, Christelle Delaite<sup>c</sup>, José-Marie Lopez-Cuesta<sup>b</sup>

<sup>a</sup> Laboratoire des Matériaux Polymères Avancés (LMPA), Université de Bejaia, 06000, Algeria

<sup>b</sup> Centre des Matériaux des Mines d'Alès (C2MA), Ecole des mines d'Alès, 6 avenue de Clavières, 30319 Alès Cedex, France<sup>1</sup>

<sup>c</sup> Laboratoire de Photochimie et d'Ingénierie Macromoléculaires (LPIM), 3b rue Alfred Werner, 68093 Mulhouse Cedex, France

## A B S T R A C T

Blends of poly(3-hydroxybutyrate-co-3-hydroxyvalerate) (PHBV) and poly(butylene succinate) (PBS) at different weight ratios (80/20, 50/50 and 20/80 w/w) and ternary PHBV/PBS/halloysite nanotubes (HNT) nanocomposites were prepared by melt compounding. Typical co-continuous and nodular morphologies were obtained with the neat blends. The effect of maleic anhydride-grafted PHBV (PHBV-g-MA) compatibilizer and HNT on the nodular microstructure and thermal properties of PHBV/PBS/HNT nanocomposites was investigated. Morphological observations using scanning electron microscopy (SEM) showed an improved dispersion of PBS nodules in the immiscible PHBV/PBS 80/20 blends, owing to the diffusion and emulsifying effect of PHBV-g-MA chains at the PHBV/PBS interface. A preferential location of HNTs in the PBS nodules was observed, due to their better wettability with PBS phase. Image analysis showed that combining HNT and compatibilizer led to a reduced emulsifying effect, attributed to the formation of PHBV-g-MA/HNT aggregates that limit the diffusion of PHBV-g-MA chains at the interface. Thermogravimetric analysis (TGA) and Pyrolysis Combustion Flow Calorimetry (PCFC) showed a better thermal stability and fire reaction of PHBV in the PHBV/PBS blends as compared to neat PHBV. Incorporation of HNT in the blends decreased their thermal stability but improved significantly their fire reaction, whereas combining PHBV-g-MA and HNT seems to level the influence of each component.

### Keywords:

Nanocomposite

Halloysite

Polymer blend

Poly(3-hydroxybutyrate-co-3-hydroxyvalerate) (PHBV)

Poly(butylene succinate) (PBS)

## 1. Introduction

The development of biobased and biodegradable polymers as potential substitutes for plastics from fossil resources is an emerging field of research and development. In recent years, different types of biodegradable polymers have attracted much attention for developing various new polymeric materials with reduced environmental impacts [1,2]. Polyhydroxyalkanoates

\* Corresponding author.

E-mail address: [nicolas.le-moigne@mines-ales.fr](mailto:nicolas.le-moigne@mines-ales.fr) (N. Le Moigne).

<sup>1</sup> C2MA is member of the European Polysaccharide Network of Excellence (EPNOE), <http://www.epnoe.eu>.

(PHAs) are derived from renewable resources and are fully biodegradable thermoplastics [3]. They are aliphatic biopolyesters naturally produced via a microbial process on sugar-based medium, and act as a source of carbon and energy storage for microorganisms [4,5].

Poly(3-hydroxybutyrate-co-3-hydroxyvalerate) (PHBV) is one of the most widely studied PHA polymers due to its potential use in packaging, automotive, biomedical, and agricultural applications because of its natural origin, biocompatibility, and thermoplastic behavior [6]. However, PHBV shows some drawbacks such as its high crystallinity and brittleness [7]. Moreover, its degradation temperature close to its melting temperature [8] makes it difficult to process. Various solutions have been proposed to solve the above problems, including physical blending, or block copolymerization [9]. Blending PHBV with other polymers such as poly(lactic acid) (PLA) [4,10], poly(butylene adipate-co-terephthalate) (PBAT) [11,12], poly(propylene carbonate) [13], poly(caprolactone) (PCL) [14] and poly(ethylene succinate) (PES) [15] represent interesting routes to control the properties of PHBV. Another polymer that can be used to blend with PHBV is poly(butylene succinate) (PBS) [16–18]. PBS is a thermoplastic polyester synthesized through the polycondensation reaction of 1,4-butanediol with succinic acid. This polymer has high flexibility, excellent impact strength, thermal and chemical resistance [19]. It can be processed easily and it is thus a good candidate for blending with PHBV. In this respect, Qiu et al. [16] blended PHBV with PBS in solution using chloroform. They reported that PHBV and PBS are immiscible and the crystallization rate of PHBV was decreased by adding PBS, although its crystallization mechanism did not change significantly. Ma et al. [17] studied the in-situ compatibilization of PHBV/PBS and PHB/PBS blends in the presence of dicumyl peroxide (DCP). During processing, DCP initiated a free-radical reaction between PHBV and PBS (and also PHB and PBS) forming PHBV-g-PBS copolymers which subsequently acted as compatibilizer and partially cross-linked networks in the blends. The size of PBS particles in PHBV or PHB decreased significantly accompanied by an improvement of the interfacial adhesion. Consequently, the mechanical properties of the PHBV/PBS and PHB/PBS blends were significantly improved.

Many strategies were developed to compatibilize polymer blends. An interesting one is the use of targeted and modified inorganic micro and nano-fillers. The effects of fillers on the morphology and structural properties of the blends vary depending on their geometry, chemical composition and modification which influence significantly their location in the blend microstructure [20]. Zembouai et al. [21] studied the effect of organomodified montmorillonite (OMMT) Cloisite 30B (C30B) with and without compatibilizer, maleic anhydride-grafted-PHBV (PHBV-g-MA), on the morphology and properties of PHBV/PLA blends prepared by melt mixing. The results showed that C30B enhances the thermal stability and improves the tensile properties of the blends such as Young's modulus. Further, a synergistic effect of compatibilizer and C30B was highlighted, leading to an improved miscibility of the two blend components. Bittmann et al. [22] investigated the properties of PHBV/PBAT blends as well as the effect of C30B on the morphology and thermal behavior of the blends. The results revealed a good dispersion of C30B in the polymer blend. They also showed that C30B enhances the thermal stability, delays the crystallization of PHBV and accelerates its melting and increases the crystallinity of PHBV. Mofokeng et al. [23] studied the morphology, thermal stability and thermal degradation kinetics of melt-mixed PHBV/PCL blends filled with titanium(IV) oxide (TiO<sub>2</sub>) nanoparticles. They showed a well dispersion of TiO<sub>2</sub> in both polymers with the presence of some aggregates. They found that the presence of TiO<sub>2</sub> enhanced the thermal stability of PHBV and PCL.

Recently, various papers have been published about the interest to incorporate halloysite (HNT) in polymer nanocomposites [24–26]. The structure and chemical composition of HNT is similar to that of kaolinite (molecular formula Al<sub>2</sub>Si<sub>2</sub>O<sub>5</sub>(OH)<sub>4</sub>·nH<sub>2</sub>O) but the unit layers in HNT are separated by a monolayer of water molecules [27–29]. HNTs have tubular microstructure with high aspect ratio and typical dimensions of 10–30 nm in inner diameter, 30–50 nm in outer diameter and 100–2000 nm in length [30,31]. HNTs are mined from natural deposits in various countries like China, New Zealand, France and Algeria [30]. Russo et al. [31] studied the thermal and structural properties of commercial PHBV/PBAT blends by varying the concentration of neat and silanized HNTs within the blends. Their investigations demonstrated that HNT increases the degree of crystallinity of PHBV whereas the crystallization of PBAT remained unchanged.

In the present study, PHBV/PBS blends at various ratios (100/0, 80/20, 50/50, 20/80, 0/100) have been prepared by melt compounding. PHBV-g-MA (prepared by melt mixing in an internal mixer using maleic anhydride and dicumyl peroxide as initiator) was used as compatibilizer for the blends. Halloysite nanotubes were added to neat and compatibilized PHBV/PBS blends. The influence of PHBV-g-MA, HNT and the combined effects of HNT and compatibilizer on the morphology, crystallization, thermal stability and flammability of PHBV/PBS blends were investigated.

## 2. Experimental section

### 2.1. Materials

An injection molding grade of PHBV containing 7 wt% of hydroxyvalerate (HV) and nucleated by boron nitride [32], was purchased from NaturePlast (France) under the trade name PHI 002. According to the manufacturer, PHBV has the following physical properties: density = 1.25 g/cm<sup>3</sup>, melting temperature  $T_m$  = 170 °C and glass transition temperature  $T_g$  = 5 °C. Poly(butylene succinate) (PBS) (Bionolle 1001MD) was supplied by Showa Denko K.K. (Japan). It has a density of 1.26 g/cm<sup>3</sup>, a crystallization temperature  $T_c$  of 80 °C and melting temperature  $T_m$  of 115 °C (determined by differential scanning calorimeter, DSC).

Algerian halloysite (HNT) was collected from the Djebel Debbagh in the region of Guelma located in the north-east of Algeria. It was supplied by SOALKA Company (Algerian Company of Kaolins). Prior to use, the stone-like raw HNT was finely ground into powder using a laboratory ball mill (FAURE Equipement SA) for 1 h and sifted through a 40  $\mu\text{m}$  sieve to obtain primary microparticles having an average diameter of 25  $\mu\text{m}$  with a nanoparticle fraction. The micrographs of HNT obtained with a scanning transmission electron microscopy detector (STEM) and scanning electron microscopy (SEM) are shown in Fig. 1. Micrographs show that halloysite is present in nanometric size range with the presence of aggregates. The specific surface area of HNT was measured using the Brunauer–Emmett–Teller (BET) method and equals 51.4  $\text{m}^2/\text{g}$ . The elemental composition of Algerian halloysite obtained with a MagiXPhilips X-ray Fluorescence Spectrometer (XRF Spectrometer) is indicated in Table 1. Algerian halloysite contains a substantial amount of  $\text{MnO}_2$  (1.88 wt%) which gives it its gray color.

## 2.2. Preparation of PHBV-g-MA compatibilizer

PHBV-g-MA was prepared by mixing 291 g of PHBV, 9 g of maleic anhydride (MA) (Sigma Aldrich) and 4.5 g of dicumyl peroxide (DCP) as initiator (Sigma Aldrich) in a HAAKE Rheomix internal mixer, according to the procedure reported by Salim et al. [33]. The rotor speed was set at 20 rpm for 3 min and increased progressively to 30 rpm for 5 min when MA and DCP were added. PHBV-g-MA was collected, ground and dried under vacuum for 6 h at 100  $^{\circ}\text{C}$  to remove any non-reacted MA. The grafting amount of MA was determined by titration using phenolphthalein as indicator according to the procedure described by Issaadi et al. [34] and Chen et al. [35]. The grafted sample ( $2.5 \pm 0.01$  g) was dissolved in 40 mL of chloroform, and 1.5 mL of 1 M hydrochloric acid was added. The solution was heated at 60  $^{\circ}\text{C}$  and stirred vigorously for 24 h. The grafted polymer was selectively recovered by precipitation into 400 mL of ethanol, followed by filtration, and dried at 100  $^{\circ}\text{C}$  for 16 h.

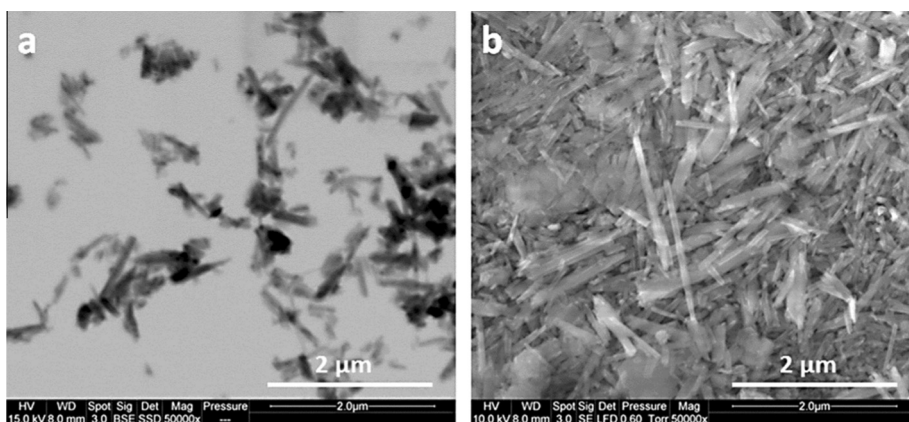


Fig. 1. STEM (a) and SEM (b) micrographs of Algerian HNT.

**Table 1**  
Elemental composition of HNT obtained by X-ray fluorescence analysis.

	Content (wt%)
$\text{SiO}_2$	40.1
$\text{Al}_2\text{O}_3$	37.4
$\text{TiO}_2$	0.03
$\text{P}_2\text{O}_5$	0.04
$\text{SO}_3$	1.72
$\text{MnO}_2$	1.88
$\text{CaO}$	0.41
$\text{NiO}$	0.08
$\text{MgO}$	0.01
$\text{Fe}_2\text{O}_3$	0.3
$\text{CoO}$	0.06
$\text{Cl}$	0.05
$\text{Na}_2\text{O}$	0.14
$\text{As}_2\text{O}_3$	0.13
$\text{BaO}$	0.07
$\text{ZnO}$	0.06
$\text{CuO}$	0.02
$\text{K}_2\text{O}$	0.33
LOI (Loss Of Ignition at 800 $^{\circ}\text{C}$ )	17.4

Samples of  $0.4 \pm 0.01$  g were completely dissolved in 40 mL of chloroform containing phenolphthalein indicator. The titration was carried out with 0.06 N of potassium hydroxide (KOH) in methanol. The percentage of MA grafting was calculated according to Eq. (1), and it was found that 1.17% of MA was grafted on PHBV.

$$\%MA = \frac{C_{KOH} \cdot V_{KOH}}{2W_{PHBV-g-MA}} 98.06 \times 100 \quad (1)$$

where  $C_{KOH}$  and  $V_{KOH}$  are the concentration and the volume of KOH solution, respectively, and  $W_{PHBV-g-MA}$  is the weight of the maleated sample.

### 2.3. Preparation of PHBV/PBS blends and PHBV/PBS/HNT nanocomposites

To minimize the moisture effect and hydrolytic degradation, pellets of PHBV, PBS and PHBV-g-MA were dried in a vacuum oven at 60 °C for 16 h and HNT was dried at 100 °C prior to compounding. PHBV/PBS blends at various ratios (100/0, 80/20, 50/50, 20/80, 0/100 w/w) were prepared using a twin-screw microcompounder (DSM Xplore, Netherlands; 15 cm<sup>3</sup> barrel volume) at 175 °C for 5 min and 40 rpm. PHBV/PBS/HNT nanocomposites with and without compatibilization were prepared by adding 5 wt% of HNT during compounding. Compatibilized PHBV/PBS blends and PHBV/PBS/HNT nanocomposites were prepared by adding 5 wt% of PHBV-g-MA during compounding. After granulating, all samples were injection-molded in a small injection molding device Zamak Mercator (Poland) and dumbbell-shaped specimens (ISO 527-2 1BA) were prepared. Blends were heated at 170 °C for 5 min in the heating chamber. The mold temperature was held constant at 60 °C and the injection pressure was set at 2 bar. The codifications and compositions of the samples are given in Table 2.

### 2.4. Structural and chemical characterization

#### 2.4.1. Scanning electron microscopy (SEM) and scanning transmission electron microscopy (STEM) observations

The morphology of cryo-fractured surfaces of the different extrudates of PHBV/PBS blends was examined using a Quanta 200 FEG (FEI Company) in environmental mode. Chloroform was used to selectively dissolve the PBS phase at room temperature for one hour. To avoid any degradation during observation, the samples surfaces were coated with carbon. SEM micrographs were analyzed with Aphelion™ 4.3.1 (ADCIS) software. The background images were first subtracted from the micrographs to remove background illumination differences by mean of opening/closing procedures. The resulting image was then binarized and PBS domains (around 2000 objects) were identified, labeled and filtered by surface area value with respect to the scale of observation. For each sample, nodule size distribution was obtained from a multi-scale analysis (from 0.004 to 0.06 μm<sup>2</sup> (scale factor 5000) and from 0.06 to 1.8 μm<sup>2</sup> (scale factor 10,000).

Scanning transmission electron microscopy (STEM) analyses were performed using a STEM detector at acceleration voltage of 5 kV to observe HNT dispersion in ultrathin sections (thickness about 70 nm) of PHBV/PBS 80/20 + HNT without and with compatibilization, which were prepared using an ultra-microtome (Leica Ultracut) equipped with a diamond knife. The ultrathin sections were cut at -80 °C and deposited on Cu grids.

#### 2.4.2. Fourier transform infrared spectroscopy (FTIR)

FTIR spectra of PHBV/PBS blends and PHBV/PBS/HNT nanocomposites were recorded on injected specimens with a BRUKER Vertex 70 spectrometer in attenuated total reflectance (ATR) mode. FTIR spectra were recorded in the range of 4000–400 cm<sup>-1</sup> with a resolution of 4 cm<sup>-1</sup> and 50 scans. All the spectra were normalized according to the band at 1450 cm<sup>-1</sup>, assigned to -CH<sub>3</sub> asymmetric group deformation.

#### 2.4.3. Nuclear magnetic resonance spectroscopy

<sup>1</sup>H and <sup>13</sup>C high-resolution one-dimensional NMR spectra were recorded at room temperature in deuterated chloroform (CDCl<sub>3</sub>) using a Bruker Avance-300 NMR spectrometer. <sup>1</sup>H NMR spectra were obtained at 400.17 MHz and an acquisition time of 3.9715 s and <sup>13</sup>C NMR spectra were obtained at 100.62 MHz and an acquisition time of 1.3631 s. Chemical shifts were referenced to the residual proton peak of CDCl<sub>3</sub> at 7.20 ppm and to the carbon peak of CDCl<sub>3</sub> at 77 ppm.

**Table 2**

Codification and composition of the different PHBV/PBS and PHBV/PBS/HNT nanocomposites blends prepared.

Samples	PHBV (wt%)	PBS (wt%)	HNT (wt%)	PHBV-g-MA (wt%)
PHBV	100	0	-	-
PBS	0	100	-	-
PHBV/PBS 80/20	80	20	-	-
PHBV/PBS 50/50	50	50	-	-
PHBV/PBS 20/80	20	80	-	-
PHBV/PBS 80/20 + PHBV-g-MA	76	19	-	5
PHBV/PBS 80/20 + HNT	76	19	5	-
PHBV/PBS 80/20 + HNT + PHBV-g-MA	72	18	5	5

#### 2.4.4. Size exclusion chromatography (SEC)

The molecular weights of PHBV were determined by size exclusion chromatography (SEC). Samples (typically 10 mg) were dissolved at a concentration of 10 mg/mL in chloroform and let under stirring for 2 min at 70 °C. Before injection, all samples were filtered through a 0.2 µm filter to remove any insoluble fractions or particles. SEC experiments were carrying out using a refractive index detector with 3 columns Agilent PLgel 5 µm (7.5 × 300 mm). The pore size of each column was 10,000 Å, 1000 Å and 500 Å, respectively. The SEC was calibrated using a mix of polystyrene standards. Chloroform was used as the eluent at a flow rate of 0.8 mL/min. The weight and number average molecular weights,  $\overline{M}_w$  and  $\overline{M}_n$  respectively, as well as the polydispersity index  $I_p$  were determined for neat PHBV and PHBV/HNT nanocomposites.

### 2.5. Thermal characterization

#### 2.5.1. Differential scanning calorimetry (DSC)

A Perkin-Elmer Diamond DSC differential scanning calorimeter (Pyris-1 DSC) equipped with an Intracooler II was used to investigate the melting and non-isothermal crystallization of the different PHBV/PBS blends and PHBV/PBS/HNT nanocomposites. The temperature and heat flow were calibrated with indium. Samples of 13 mg were encapsulated in aluminum pans and heated from -50 °C to 200 °C at a heating and cooling rate of 10 °C/min using nitrogen as purge gas. The thermal history of the samples was erased by a preliminary heating (-50 °C to 200 °C range). The measurements were made from the first cooling scan and the second heating scan. At least two measurements were performed for each sample to ensure repeatability. The degree of crystallinity ( $X_c$ ) of PHBV and PBS in their blends was determined from the second melting enthalpy values according to Eq. (2):

$$X_c = \frac{\Delta H_m}{f_p \times \Delta H_m^0} \times 100 \quad (2)$$

where  $\Delta H_m$  (J/g) is the second melting enthalpy of the polymer matrix,  $f_p$  is the polymer weight fraction of PHBV or PBS in the sample and  $\Delta H_m^0$  is the melting enthalpy of pure crystalline PHBV ( $\Delta H_m^0 = 146$  J/g) [36] or PBS ( $\Delta H_m^0 = 200$  J/g) [37].

#### 2.5.2. Thermogravimetric Analysis (TGA)

Thermal stability of various samples was performed using a TGA apparatus (SETSYS, Setaram, France). The sample weight was approximately 15 mg. Experiments were performed in the temperature range 30–650 °C at a heating rate of 10 °C/min under nitrogen atmosphere. The initial decomposition temperatures were determined at 5% and 10% of weight loss. The maximum degradation rate temperature was measured at the DTG peak maximum, and the residue left at 600 °C was determined for all the samples.

#### 2.5.3. Pyrolysis Combustion Flow Calorimeter (PCFC)

Flammability of the different blends and nanocomposites was investigated using a pyrolysis combustion flow calorimeter (PCFC) (Fire Testing Technology). This technique was firstly developed by Lyon and Walters [38] in order to study the thermal degradation of samples at the microscopic scale. Sample weights are around  $2 \pm 0.5$  mg. Samples are first pyrolyzed at 1 °C/s and the volatile thermal degradation products are swept from a pyrolysis chamber by an inert gas and combined with excess oxygen in a tubular furnace at flame temperatures to force complete combustion. Heat Release Rate (HRR) is measured as function of temperature. This enables to determine the peak value of HRR as well as the Total Heat Release THR (area below the HRR curve). The effective heat capacity corresponds to the Heat Release/Mass Loss ratio. An average value of three repeated tests was taken for each composition.

## 3. Results and discussion

### 3.1. Structural analysis by SEM

#### 3.1.1. Morphology of PHBV/PBS blends

SEM analysis was used to investigate the morphology of neat polymers and the different PHBV/PBS blends. Fig. 2a and b shows SEM images of the cryo-fractured surfaces for neat PHBV and neat PBS, respectively. Neat PHBV shows an irregular surface due to its crystalline structure [10], whereas PBS exhibits a smoother one. Phase morphology of the blends was identified after selective dissolution of PBS using chloroform at room temperature for 1 h. For the PHBV/PBS blend at 80/20% w/w, the holes correspond to the extracted PBS and reveal a nodular structure (Fig. 2c). A co-continuous structure was observed at 50 wt% of PBS in PHBV (Fig. 2d). Similar microstructures were observed by Ma et al. [39] for PHB/PBS blends. Based on these results, the effect of HNTs and the PHBV-g-MA compatibilizer was investigated on PHBV/PBS 80/20 blend so as to analyze their potential compatibilizing effect on the nodular structure.

#### 3.1.2. Effect of PHBV-g-MA and HNTs on the nodular structure of PHBV/PBS blend

SEM micrographs after selective etching of PBS for the PHBV/PBS 80/20 blend with 5 wt% of PHBV-g-MA, 5 wt% of HNT and combining PHBV-g-MA and HNT are shown in Fig. 3. Adding 5 wt% of PHBV-g-MA (Fig. 3b) refined greatly the nodular

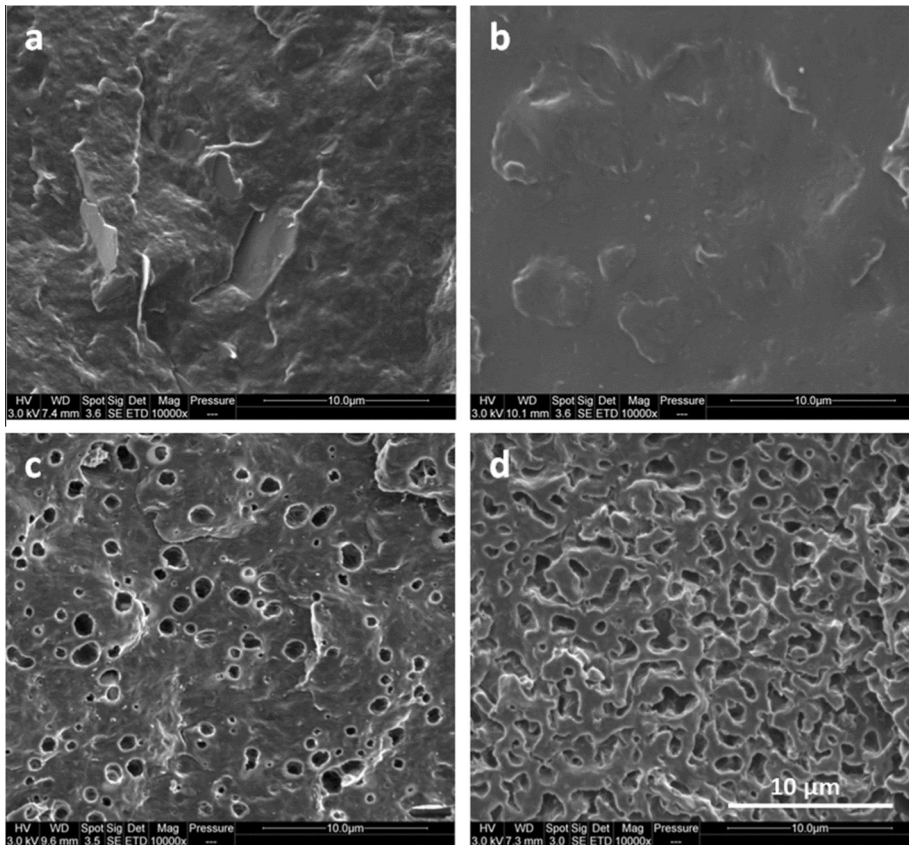


**Fig. 2.** SEM micrographs of cryo-fractured surfaces of neat PHBV (a), neat PBS (b) and PHBV/PBS blends after selective etching of PBS with chloroform, 80/20 w/w (c), 50/50 w/w (d). Holes correspond to the PBS nodules.

morphology of PHBV/PBS 80/20 blend (Fig. 3a). The PBS droplet sizes are noticeably reduced, and this reduction may be attributed to the formation of an interphase resulting from the migration of PHBV-g-MA chains to the PHBV/PBS interfacial zone which reduces the interfacial tension between PHBV and PBS. A significant emulsifying effect is thus obtained with the presence of PHBV-g-MA in the PHBV/PBS 80/20 blend.

With the presence of HNT, the ternary PHBV/PBS 80/20 nanocomposite still exhibit a nodular structure with fewer large PBS nodules and higher amount of small PBS nodules (Fig. 3c). The structure and final properties of nanocomposites blends are known to be widely determined by the location of nanoparticles in the blends [20]. Location of HNTs in the PHBV/PBS blend with and without PHBV-g-MA compatibilizer was thus investigated by SEM analysis (Fig. 4) at high magnification. A preferential location of HNT in the PBS phase instead of PHBV one was expected and indeed observed (Fig. 4a). The same observations were made in presence of PHBV-g-MA (Fig. 4b). According to literature, the surface tension of PBS is about 53.1 mN/m [40] and that of PHBV is about 42 mN/m [41]. Considering that the mixing time was sufficient for the thermodynamics and physical chemical interactions to be primarily responsible for the structuration of the nanocomposite blends [20], this difference in surface tension of 11 mN/m may cause the preferential migration of a part of the HNTs in PBS nodules during mixing, due to the better wettability of high surface tension HNT nanoparticles with the PBS phase that has the highest surface tension. The presence of HNTs within the PBS nodules should increase the viscosity of the PBS droplets during processing and hence limits their further coalescence, resulting in a slightly more refined structure for ternary PHBV/PBS 80/20 nanocomposite.

The morphology of the PHBV/PBS blend with adding together 5 wt% of HNT and 5 wt% of PHBV-g-MA looks like the one of the ternary PHBV/PBS/HNT nanocomposites, showing a nodular structure with similar PBS nodule sizes (Fig. 3d). The emulsifying effect of PHBV-g-MA was thus significantly reduced in the presence of HNTs, which can be attributed to a restricted molecular mobility and diffusion of PHBV-g-MA chains at the PHBV/PBS interface due to their potential interactions with HNTs.

### 3.1.3. Image analysis of PBS nodules distribution from SEM micrographs

In order to quantify the compatibilizing effect of PHBV-g-MA, HNT and combining PHBV-g-MA and HNT on the morphology of PHBV/PBS 80/20 blends, image analysis was performed on SEM micrographs of selectively etched surfaces for each

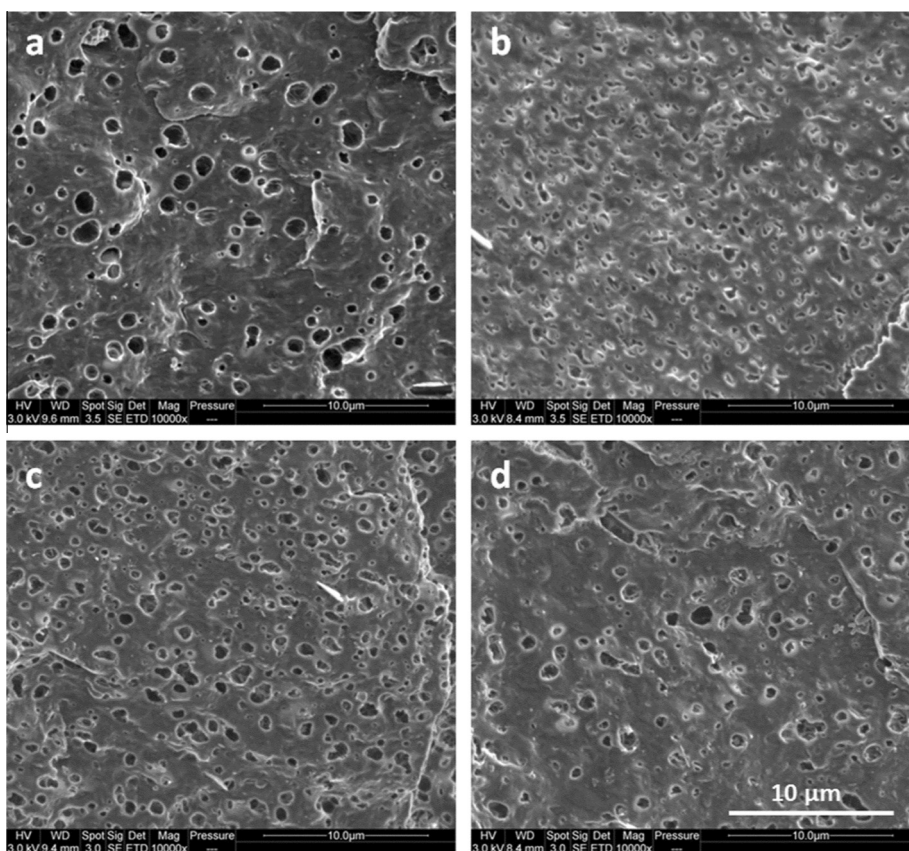


**Fig. 3.** SEM micrographs of PHBV/PBS 80/20 (a), PHBV/PBS 80/20 with 5 wt% of PHBV-g-MA (b), 5 wt% of HNT (c) and combining PHBV-g-MA and HNT (d), after selective etching of PBS with chloroform. Holes correspond to the PBS nodules.

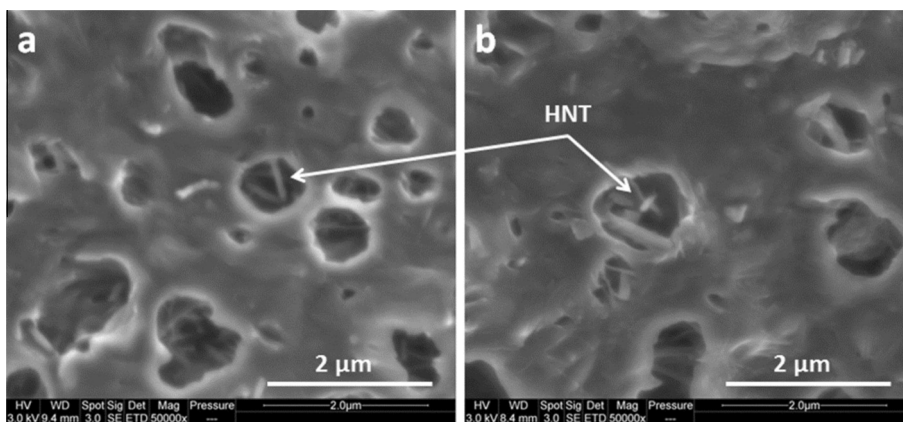


**Fig. 4.** SEM micrographs of PHBV/PBS 80/20 with 5 wt% of HNT (a) and combining 5 wt% of PHBV-g-MA and 5 wt% of HNT (after selective etching of PBS with chloroform).

sample. The resulting area distributions number weighted of the PBS nodules are shown in Fig. 5. The median nodule area for the neat PHBV/PBS 80/20 blend was  $0.240 \mu\text{m}^2$  with many large nodules having areas up to  $1.724 \mu\text{m}^2$ . For the PHBV/PBS 80/20 blend compatibilized with PHBV-g-MA, the area distribution was considerably modified with a median nodule area of  $0.041 \mu\text{m}^2$  and minimum nodule areas that reached  $0.004 \mu\text{m}^2$ . As can be seen, the distribution is very narrow and centered on the median value with very low upper quartile and decile values of  $0.088 \mu\text{m}^2$  and  $0.157 \mu\text{m}^2$ , respectively. This result is thus in accordance with the SEM observations and attests for the marked emulsifying effect of PHBV-g-MA and the homogenization of the PBS nodules size within the blend. The addition of HNTs to the PHBV/PBS 80/20 blend also

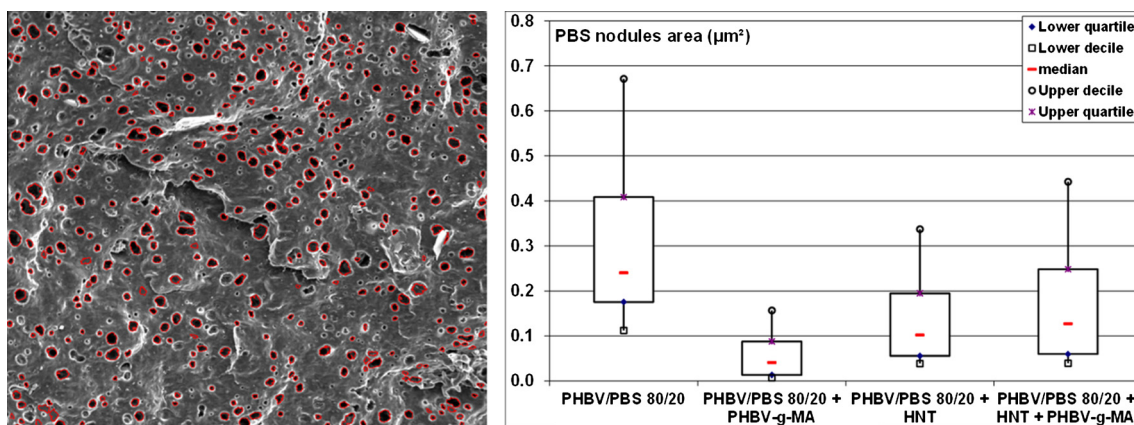


**Fig. 5.** Example of PBS nodules detection by image analysis on SEM micrographs of PHBV/PBS 80/20 blend (left), and box plots of area distributions number weighted of PBS nodules for PHBV/PBS 80/20 blend and PHBV/PBS/HNT nanocomposites with and without PHBV-g-MA compatibilization (right).

induced a significant reduction of the median nodule area which is  $0.102 \mu\text{m}^2$ . Furthermore, a substantial reduction of the large nodules was observed with upper quartile and decile values of  $0.195 \mu\text{m}^2$  and  $0.337 \mu\text{m}^2$ , respectively. This supports the SEM observations and the assumption of a restricted coalescence of PBS nodules in the presence of HNTs. When combining PHBV-g-MA and HNT, a similar area distribution of the PBS nodules is observed as compared to the filled and non-compatible blend with median and upper quartile and decile values of  $0.127 \mu\text{m}^2$ ,  $0.248 \mu\text{m}^2$  and  $0.443 \mu\text{m}^2$ , respectively. This result confirms the limited emulsifying of the PHBV-g-MA in the presence of HNTs due to their potential interactions that should impede the diffusion of a part of PHBV-g-MA chains at the PHBV/PBS interface.

#### 3.1.4. HNT dispersion within the nodular PHBV/PBS blend

SEM and STEM observations were achieved to study the dispersion of HNTs in PHBV/PBS 80/20 + HNT with and without PHBV-g-MA compatibilization (Fig. 6). For both ternary PHBV/PBS/HNT blends, individually dispersed HNTs were observed (Fig. 6c and d), in addition with few large aggregates or rather primary micrometric particles of 2–10  $\mu\text{m}$  in diameter (Fig. 6a and b). This result shows that the grinding and processing conditions used allowed obtaining a good dispersion of HNTs within the PHBV/PBS blends down to the nanometric scale. It seems like more HNT aggregates of about 500 nm (Fig. 6b) were produced in the presence of PHBV-g-MA, which supports the occurrence of interactions between the surface hydroxyl groups of HNT and acidic groups of PHBV-g-MA to form PHBV-g-MA/HNT aggregates. As postulated above, these interactions should hinder the migration of PHBV-g-MA chains at the PHBV/PBS interface, hence limiting the emulsifying effect of PHBV-g-MA.

### 3.2. Physical chemical interactions and chemical structure

#### 3.2.1. Fourier-transform infrared spectroscopy (FTIR) analysis

The FTIR analysis was performed to identify the physical and chemical interactions between the neat polymers during melt blending. The ATR-FTIR spectra of neat PHBV, neat PBS and their different blends are shown in Fig. 7. For neat PHBV, absorption bands at  $2932 \text{ cm}^{-1}$  and  $1451 \text{ cm}^{-1}$  were attributed to  $-\text{CH}$  stretching. The presence of absorption band at  $2975 \text{ cm}^{-1}$  is attributed to  $\text{C}-\text{H}$  stretching vibration of crystalline phase of PHBV [42]. A strong and sharp absorption band at  $1719 \text{ cm}^{-1}$  is observed which is assigned to the  $\text{C}=\text{O}$  stretching mode of the crystalline parts in PHBV [43]. Band at  $1451 \text{ cm}^{-1}$  is caused by  $\text{CH}_3$  asymmetric deformation [44,45]. In addition, the peaks at 1275, 1261, and  $1226 \text{ cm}^{-1}$  are assigned to the  $\text{C}-\text{O}-\text{C}$  stretching modes of the crystalline parts. The peak detected near  $1180 \text{ cm}^{-1}$  is attributed to the amorphous state of  $\text{C}-\text{O}-\text{C}$  stretching band. For neat PBS, the absorption band related to  $-\text{CH}$  stretching,  $\text{C}-\text{H}$  stretching vibration and  $\text{C}=\text{O}$  stretching vibration are observed at  $2963 \text{ cm}^{-1}$ ,  $2921 \text{ cm}^{-1}$  and  $1710 \text{ cm}^{-1}$ , respectively. The absorption band at  $1046 \text{ cm}^{-1}$  is due to  $-\text{O}-\text{C}-\text{C}-$  stretching vibration in PBS. The peak at  $1155 \text{ cm}^{-1}$  is assigned to the stretching of the  $-\text{C}-\text{O}-\text{C}-$  group in the ester linkages of PBS.

The FTIR spectra of PHBV/PBS blends recorded in the region  $1800-1600 \text{ cm}^{-1}$  are shown in Fig. 7. The carbonyl absorption bands show modification in shape and intensity depending on the blend composition. It is interesting to note that the characteristic band for crystalline parts in PHBV, positioned at  $1719 \text{ cm}^{-1}$ , gradually increases with the increase of PBS content (Fig. 7b). The peak of carbonyl group in the blends is also slightly shifted to lower wavenumbers, when the content ratio of PBS increases. The other bands remain unchanged.

The FTIR spectra of PHBV/PBS 80/20 and its HNT based nanocomposites with and without compatibilizer as well as those of neat PHBV-g-MA and HNT are presented in Fig. 7c. The spectrum of HNT exhibits two intense bands at  $3621$  and  $3694 \text{ cm}^{-1}$ , which are assigned to the  $\text{O}-\text{H}$  group vibration. The interlayer water is indicated by the stretching vibration

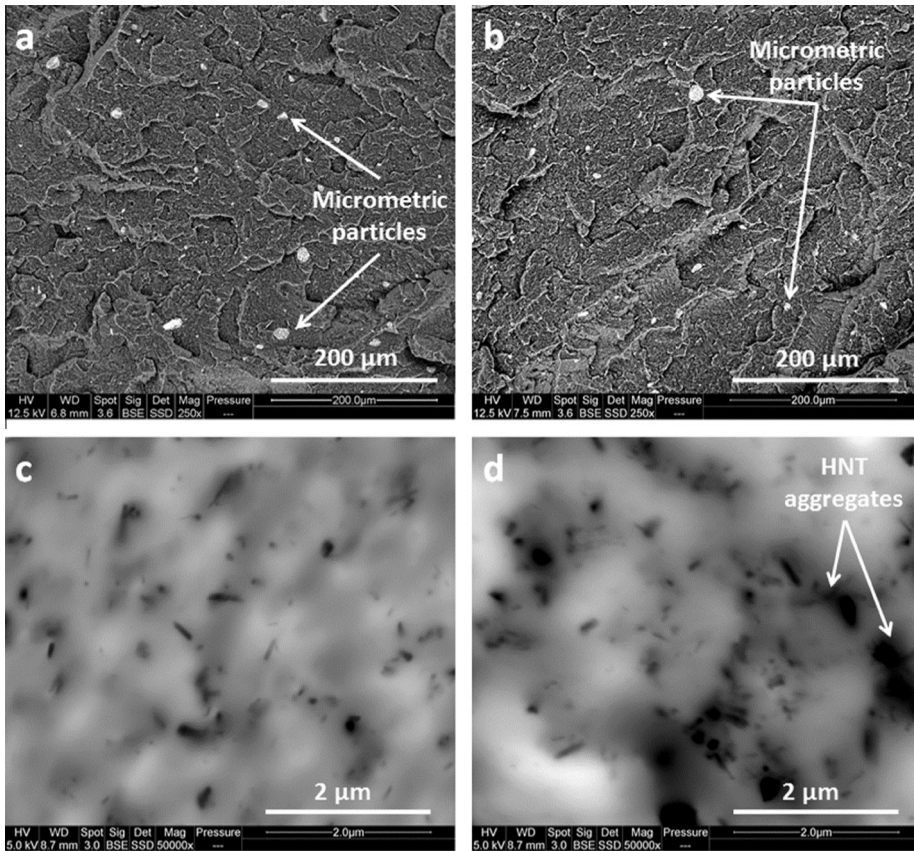


**Fig. 6.** SEM micrographs of cryo-fractured surfaces of PHBV/PBS/HNT 80/20 nanocomposites (a) without and (b) with PHBV-g-MA; and STEM micrographs of ultrathin sections of PHBV/PBS/HNT 80/20 nanocomposites (c) without and (d) with PHBV-g-MA.

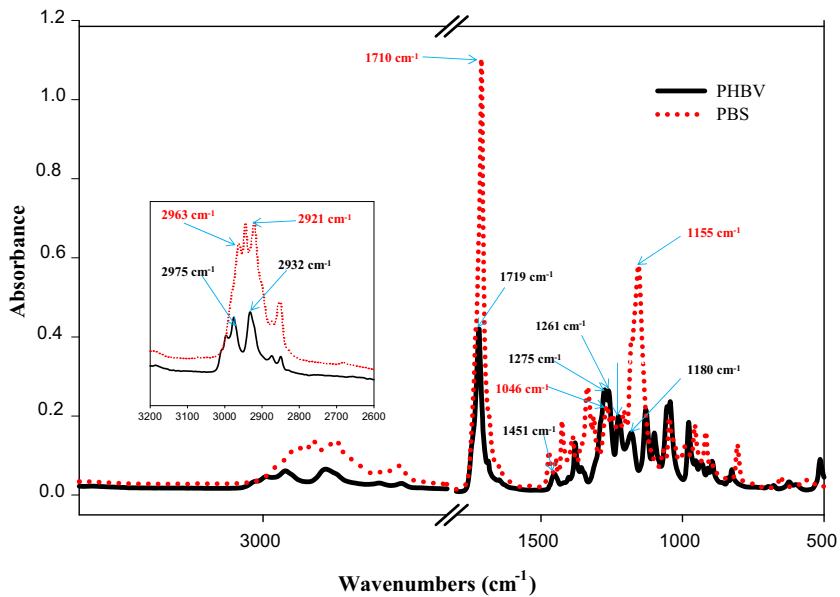


**Fig. 7a.** FTIR spectra of neat PHBV and neat PBS recorded in the region 4000–500  $\text{cm}^{-1}$ .

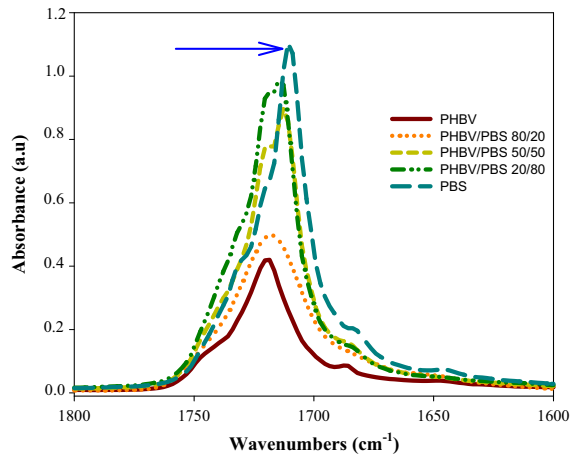


**Fig. 7b.** FTIR spectra of the carbonyl region ( $1800\text{--}1600\text{ cm}^{-1}$ ) for PHBV, PBS and various PHBV/PBS blends.

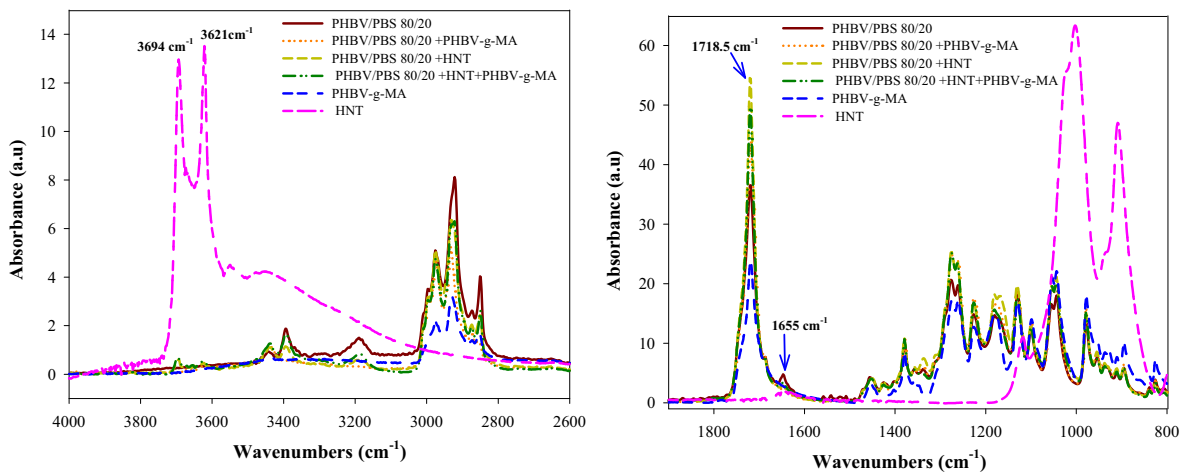


**Fig. 7c.** FTIR spectra in the range  $4000\text{--}2600\text{ cm}^{-1}$  and  $1900\text{--}800\text{ cm}^{-1}$  of PHBV/PBS 80/20 binary blend and PHBV/PBS/HNT nanocomposites with and without PHBV-g-MA compatibilization.

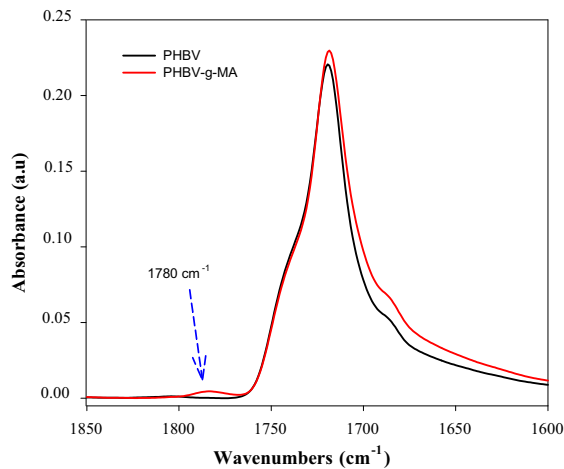


**Fig. 7d.** FTIR spectra in the range  $1850\text{--}1600\text{ cm}^{-1}$  of PHBV and PHBV-g-MA.

bands at  $1655\text{ cm}^{-1}$ . The grafting reaction of MA was monitored by FT-IR analysis. A new absorption band centered at  $1780\text{ cm}^{-1}$  appeared in the spectra of PHBV-g-MA (Fig. 7d). This band is attributed to the symmetric C=O stretching bonds of MA [34,46], thus confirming that grafting reaction occurred.

These bands are also present in the PHBV/PBS 80/20 with HNT (with and without compatibilization). It is interesting to note that there is no new absorption bands or peak shifts appearing with respect to the individual spectra of the blend components. This suggests that there are no specific chemical or physical interactions created in the ternary nanocomposite systems, or at least not detectable by FTIR. The spectrum of blends containing PHBV-g-MA was also dominated by the characteristic signals of PHBV and PBS.

It should be mentioned that a significant increase of the carbonyl band intensity (at  $1718.5\text{ cm}^{-1}$ ) is observed when adding HNT with and without PHBV-g-MA. This is explained by the degradation of PHBV, and possibly PBS, in the presence of HNT. SEC measurements conducted on neat PHBV and PHBV/HNT nanocomposite revealed a decrease of roughly 20% for both  $\overline{M}_w$  and  $\overline{M}_n$ , from 316,430 g/mol to 262,515 g/mol and 123,990 g/mol to 95,735 g/mol, respectively. The ester linkage of biopolyesters is indeed known to be sensitive to the presence of Al Lewis and Brønsted acid sites in the inorganic layers of silicates which catalyze its hydrolysis [47,48].

### 3.2.2. $^{13}\text{C}$ and $^1\text{H}$ NMR spectra

The chemical structure of PHBV, PBS and PHBV/PBS 80/20 blends was also investigated by  $^1\text{H}$  and  $^{13}\text{C}$  NMR (Fig. 8a–d). In the  $^1\text{H}$  NMR of PHBV (Fig. 8a) chemical shift values ranging from 0.83 ppm represent the protons of methyl terminal group of hydroxyvalerate group (V4). Chemical shift values at 1.18–1.21 ppm, 1.63 ppm, 2.38–2.43, 2.1–2.57 ppm 5.18–5.20 refer to methyl group of hydroxybutyrate group (B3), internal  $-\text{CH}_2$  group of hydroxyvalerate group (V3),  $-\text{CH}_2$  groups (V1, B1) and  $-\text{CH}$  groups, respectively. Characteristic peaks of PBS appear in the spectra of PBS as shown in Fig. 8a. Chemical shift at 1.63 ppm, 2.56 ppm and 4.05 ppm represent the H2, H3 and H1, respectively.  $^{13}\text{C}$  NMR spectra of PHBV and PBS are shown in Fig. 8b. The characteristic peak of PHBV located at 169.14 ppm is attributed to carbonyl groups ( $-\text{C}=\text{O}$ ) in the 3-hydroxybutyrate (B0) and 3-hydroxyvalerate (V0) units. The peak at 67.61 ppm is assigned to ( $-\text{CH}-$ ) group (B2). Peaks at 40.78 ppm, 29.69 ppm, 19.78 ppm and 9.36 ppm are attributed to ( $-\text{CH}_2$ ) noted B2, ( $-\text{CH}_2$ ) group, noted V3, methyl group (B3) and V4, respectively.  $^{13}\text{C}$  NMR of PBS has the following signals: 172.31 ppm, 64.18 ppm, 29.02 ppm and 25.21 ppm attributed to C3, C4, C1 and C2, respectively.

Fig. 8c and d shows the  $^1\text{H}$  and  $^{13}\text{C}$ , respectively, of PHBV/PBS 80/20, neat PHBV and PBS.  $^{13}\text{C}$  NMR peaks appearing at 169.15 ppm, 67.61 ppm, 40.78 ppm, 29.70 ppm, 19.76 ppm and 9.36 ppm are assigned to the PHBV component, while the peaks at 172.30 ppm, 29.02 ppm and 25.21 ppm are assigned to the PBS component. In the  $^1\text{H}$  NMR (Fig. 8d), all chemical shift values represent components of each polymer. It is clearly seen that the chemical shift of the PHBV/PBS 80/20 is still unchanged compared with neat polymers.

Fig. 8e and f displays  $^1\text{H}$  and  $^{13}\text{C}$  NMR spectra of PHBV/PBS 80/20 blend, and its HNT based nanocomposites with and without compatibilizer. It can be observed that  $^1\text{H}$  and  $^{13}\text{C}$  NMR spectra exhibit the same chemical shift as neat PHBV/PBS 80/20 for all formulations.

Based on FTIR and NMR analysis, it was thus not possible to observe significant shift or appearance of new peaks, which would be a proof of specific interactions occurring between the components in the ternary nanocomposites. This might be explained by the low amounts of HNTs and PHBV-g-MA within the system that does not allow detecting such variations.

## 3.3. Thermal properties

### 3.3.1. DSC analysis

Fig. 9 shows the DSC thermograms of neat PHBV, neat PBS and the different blends derived from the cooling scan and the second heating scan. The results are summarized in Table 3. It is observed that neat PHBV exhibits a crystallization peak ( $T_c$ ) at around  $116\text{ }^\circ\text{C}$ , an endothermic melting point ( $T_m$ ) at  $169\text{ }^\circ\text{C}$  and a degree of crystallinity ( $X_c$ ) of 56.8%. Neat PBS shows a  $T_c$  at around  $80\text{ }^\circ\text{C}$  and  $X_c$  of 30.5%. It is observed that PBS exhibits two endothermic peaks denoted  $T_{m1}$  and  $T_{m2}$  at  $102\text{ }^\circ\text{C}$  and  $113.5\text{ }^\circ\text{C}$ , respectively. The multiple melting behavior of PBS as observed by DSC was already reported [16,49,50] and is believed to be due to a melting and recrystallization mechanism. Because PHBV and PBS are semi-crystalline polymers, only small fluctuations corresponding to their glass transitions ( $T_g$ ) were detected on thermograms (Fig. 9). Two distinct glass transitions were observed for PBS (at around  $-35\text{ }^\circ\text{C}$ ) and PHBV (at around  $0\text{ }^\circ\text{C}$ ), attesting for the immiscibility of the two polymers in the blends [16,17]. However, for the 80/20 PHBV/PBS nodular blend, the glass transition of PBS was not detectable. This was attributed to the crystallinity of PBS, its low amount within the blend and possible interactions between PHBV and PBS chains when PBS is the minor phase.

Since PHBV and PBS are immiscible, crystallization and melting peaks of each component should also appear distinctly in the blends' thermograms. For blend compositions for which the amount of PHBV is greater than or equal to 50 wt% (Fig. 9a), the PHBV crystallization peak is noticeable and shifted to lower temperatures when the amount of PBS increases, i.e.  $107.7\text{ }^\circ\text{C}$  for the PHBV/PBS 50/50 blend. Similar observation has also been reported on PHB/PBS blends [51]. The decrease in  $T_c$  of PHBV may be the result of physical restrictions to the nucleation and growth of PHBV crystallites by the PBS domains. Further, it can be noticed for the PHBV/PBS 80/20 blend, a weak crystallization peak of PBS at low temperature (around  $48\text{ }^\circ\text{C}$ ), and the absence of characteristic crystallization peak of PHBV for PHBV/PBS 20/80 blend. These results suggest that when PBS or

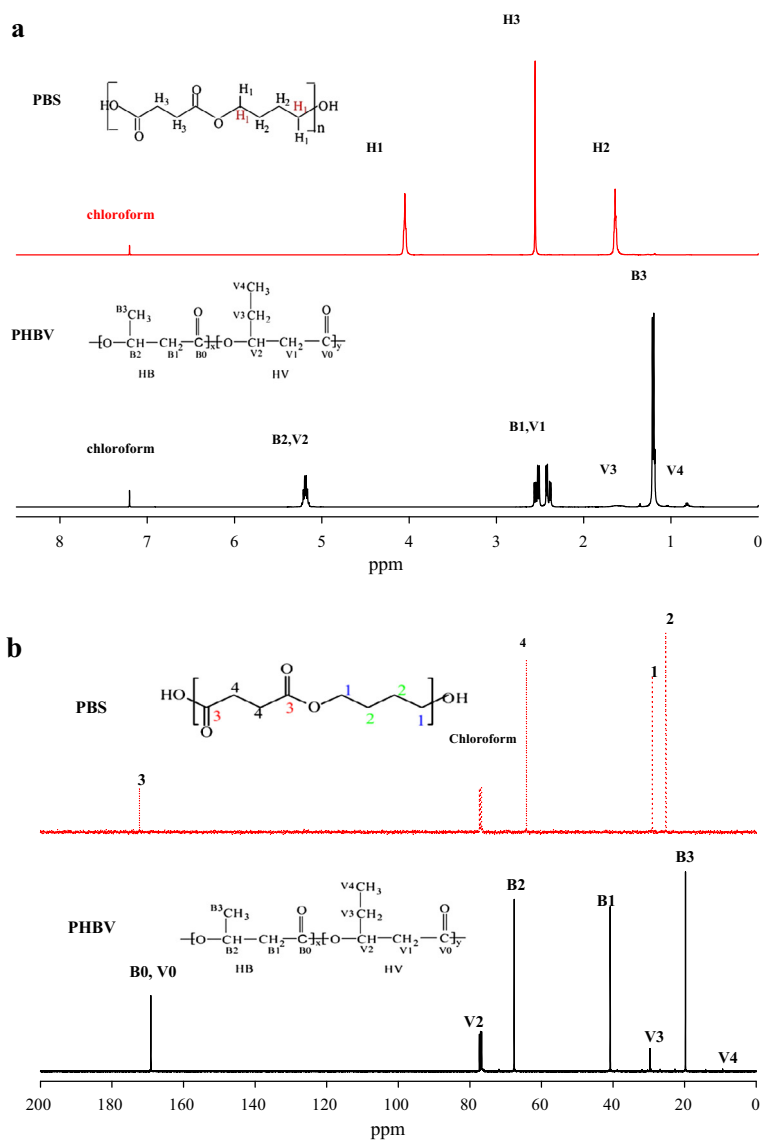


**Fig. 8.** (a, c, e)  $^1\text{H}$  NMR and (b, d, f)  $^{13}\text{C}$  NMR spectra of neat PHBV, neat PBS and PHBV/PBS 80/20 binary blend and PHBV/PBS/HNT nanocomposites.

PHBV are the minor phases within the blends, crystallization of the chains is restricted and/or occurs in the same temperature range for these particular blends. In the case of PHBV/PBS 80/20 blend,  $T_g$  of PBS was not easily detectable and  $T_c$  of both PBS and PHBV were decreased, attesting for possible interactions between PHBV and PBS chains that could restrict their molecular mobility. Besides, a restricted crystallization of PHBV in the presence of PBS was already reported in literature [18]. For PHBV/PBS 80/20 blend, migration of PHBV nuclei to the major and still molten PBS phase may also have occurred, hence limiting the nucleation in the PHBV nodules and decreasing its  $T_c$  [52].

Two separate melting peaks can be found in Fig. 9b for all PHBV/PBS blends that correspond to the melting temperatures ( $T_m$ ) of PBS and PHBV, indicating that the melting behavior of each component was not influenced significantly by the crystallization mechanism during cooling. The variations in the melting temperature of PHBV when adding PBS in the blend are indeed not very important. However, it should be mentioned that the first melting peak of PBS was not observed when PBS was added at 20 wt% and 80 wt% in the blend, suggesting that crystals of lower thermal stability were produced in this blend.

The degree of crystallinity of both PHBV and PBS were calculated from the second melting step and normalized with respect to the composition of each component in the blend. The values of  $X_c$  for PHBV and PBS in the blends are summarized in Table 3. The degree of crystallinity of PHBV for the 80/20 and 50/50 blends is lower than that of neat PHBV, and it is significantly decreased for 20/80 blend, which supports a restricted crystallization of PHBV when it is in minor amount in PBS. The degree of crystallinity of PBS slightly decreased in the presence of PHBV. The PBS crystallization was therefore slightly

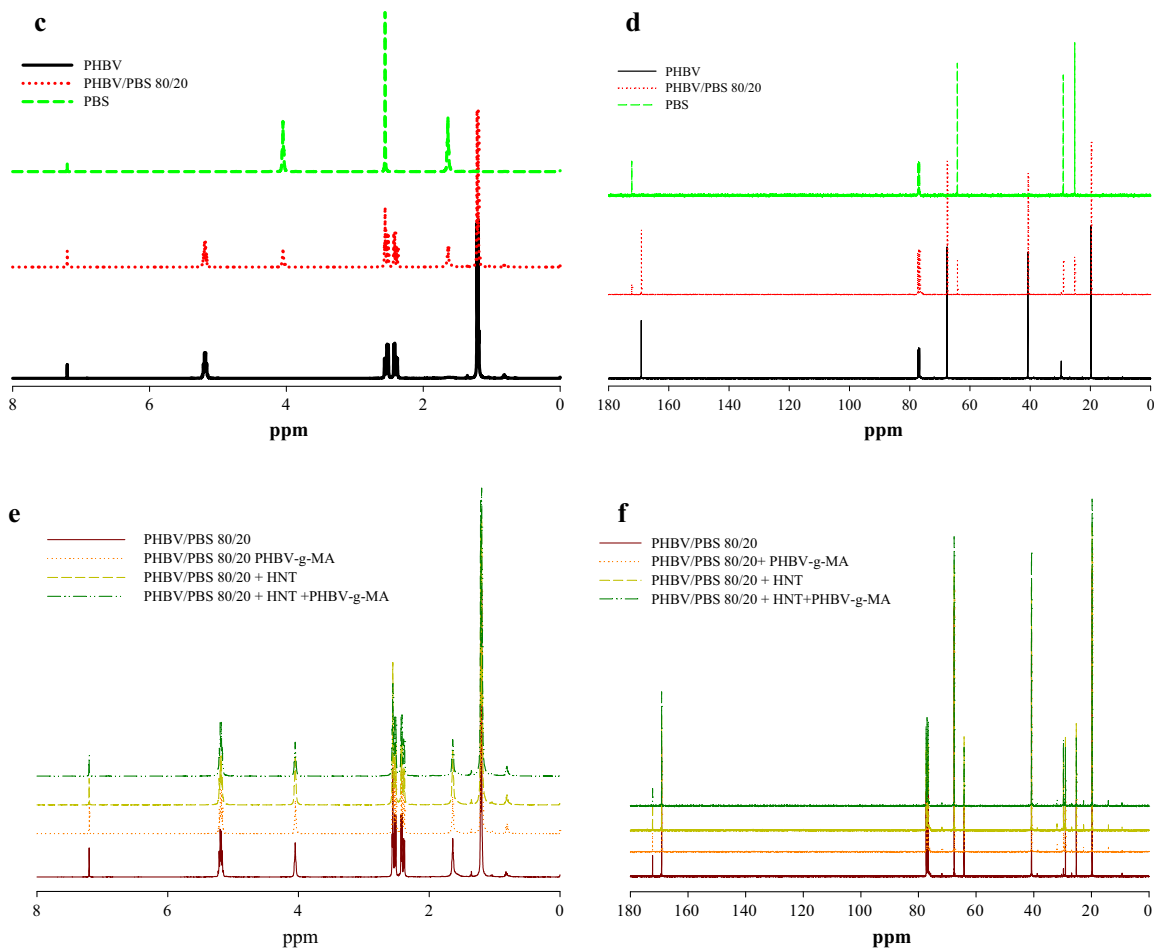


Fig. 8 (continued)

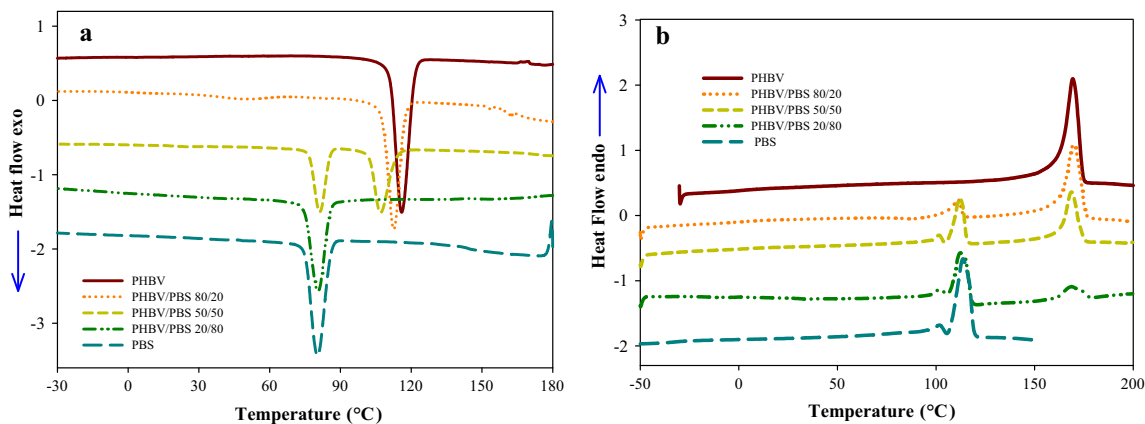


Fig. 9. DSC thermograms of neat PHBV, neat PBS and various PHBV/PBS: (a) cooling and (b) heating.

affected by the presence of PHBV, even at large PHBV amount. These results are in accordance with the work of Qiu et al. [16]. The authors indeed found that neither the crystallization rate nor the crystallization mechanisms of PBS were changed in the presence of PHBV.

As shown in Fig. 10, the incorporation of PHBV-g-MA at 5 wt% in the 80/20 blend does not involve any appreciable changes in melting and crystallization temperatures and enthalpies of PHBV (Table 4). In the presence of 5 wt% HNT, a

**Table 3**

Thermal Properties of neat PHBV, neat PBS, and PHBV/PBS Blends obtained from the cooling scan and the second heating scan.

Samples	PHBV						PBS						
	$T_c$ (°C)	$\Delta H_c$ (J/g)	$T_m$ (°C)	$\Delta H_m$ (J/g)	$T_g$ (°C)	$X_c$ (%)	$T_c$ (°C)	$\Delta H_c$ (J/g)	$T_{m1}$ (°C)	$T_{m2}$ (°C)	$\Delta H_m$ (J/g)	$T_g$ (°C)	$X_c$ (%)
PHBV	115.7 ± 0.2	83.6 ± 0.8	169.5 ± 0.2	83.0 ± 1.1	2.1 ± 0.7	56.8 ± 0.0	–	–	–	–	–	–	–
PHBV/PBS 80/20	113.2 ± 0.6	64.2 ± 0.3	170.5 ± 0.4	61.3 ± 2.6	1.3 ± 2.3	51.5 ± 0.0	48.4 ± 0.3	3.5 ± 0.21	–	111.4 ± 0.2	10.7 ± 0.2	–	26.8 ± 0.0
PHBV/PBS 50/50	107.7 ± 0.6	37.2 ± 0.4	168.4 ± 0.2	36.7 ± 0.1	–1.4 ± 0.4	50.1 ± 0.0	81.9 ± 0.6	28.2 ± 1.02	101.5 ± 0.43	111.9 ± 0.2	26.6 ± 1.0	–36.6 ± 0.6	26.6 ± 0.0
PHBV/PBS 20/80	–	–	170.5 ± 2	12.7 ± 0.5	–1.8 ± 0.7	43.5 ± 0.0	81.8 ± 1.2	49.8 ± 1.9	101.7 ± 0.14	112.4 ± 1	38.7 ± 1.9	–33.4 ± 1.1	24.2 ± 0.0
PBS	–	–	–	–	–	–	79.3 ± 1.5	62.6 ± 0.1	101.8 ± 0.5	113.5 ± 0.3	61.1 ± 0.06	–33.6 ± 1.0	30.5 ± 0.01

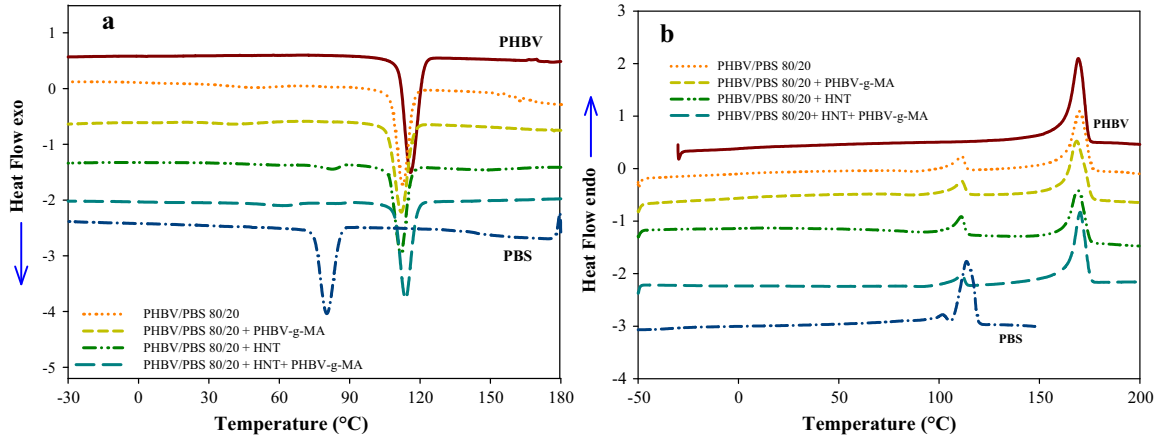


**Fig. 10.** DSC thermograms of PHBV/PBS 80/20 binary blend and PHBV/PBS/HNT nanocomposites with and without PHBV-g-MA compatibilization: (a) cooling scan and (b) heating scan.

decreased enthalpy of crystallization ( $\Delta H_c$ ) and melting ( $\Delta H_m$ ) of PHBV were observed, accompanied by lower crystallization temperature and degree of crystallinity. This suggests that HNTs restrict the crystallization of PHBV in PHBV/PBS blends. Conversely, incorporating HNT in the 80/20 blend increases significantly the crystallization temperature and the degree of crystallinity  $X_c$  of PBS, i.e. 83 °C and 31.2% as compared to 48 °C and 26.8% for 80/20 blend, respectively. Based on these observations, it is postulated that HNTs act as nucleating agents for PBS, favored by their preferential localization in PBS nodules.

When combining PHBV-g-MA with HNT in the blend, an interesting behavior is observed. PHBV presents similar behavior as in the unfilled and non-compatibilized 80/20 blend, meaning that the presence of PHBV-g-MA prevents the negative effect of HNTs on the crystallization of PHBV. Conversely, PHBV-g-MA with HNTs tends to inhibit the crystallization of PBS. These two phenomena suggest that PHBV-g-MA limits the direct PHBV/HNT and PBS/HNT interactions, and hence support the assumption that PHBV-g-MA/HNT aggregates are formed.

### 3.3.2. Thermogravimetric analysis (TGA)

TGA and scans of neat PHBV, PBS and PHBV/PBS blends at different ratios are presented in Fig. 11a and b, respectively. The onset decomposition temperature (temperature at 5 and 10 wt% loss), temperature at 50 wt% loss and peak decomposition temperatures ( $T_{max}$ ), of the respective blend compositions are given in Table 5. The DTG curves for PHBV/PBS blends in Fig. 11b show the temperatures of decomposition of PHBV and PBS in the blends.

Neat polymers show single step decomposition in the nitrogen atmosphere. PHBV starts degrading at around 271 °C, PBS is more thermally stable and its degradation starts at around 358 °C. The immiscible polymer blends show two degradation steps, the first one associated to their PHBV fraction and the second one related to their PBS fraction.

In order to find out whether interactions between the components of the blends occur, the theoretical TGA curves of the blends were constructed from the experimental TGA curves of the pure components assuming no interactions. Theoretical TGA curves were calculated according to Eq. (3):

$$M_{blend} = W_{PHBV}M_{PHBV} + W_{PBS}M_{PBS} \quad (3)$$

where  $M_{PHBV}$  is the mass loss of neat PHBV,  $M_{PBS}$  is the mass loss of neat PBS,  $W_{PHBV}$  and  $W_{PBS}$  are the respective polymer weight fractions in the blends.

Fig. 11c shows experimental and theoretical TGA curves of PHBV/PBS binary blends. It can be observed that for all blends, thermal decomposition of PHBV is shifted to higher temperature. However, it is observed an important negative deviation between the experimental and theoretical curves of PBS, meaning that the thermal stability of PBS in the blends is reduced. It is thus evidenced that blending PHBV and PBS confers a higher thermal stability for PHBV, but a lower thermal stability for PBS. Similar results were found by Mofokeng et al. [23] for PHBV/PCL blends.

Influence of the addition of PHBV-g-MA as compatibilizer, HNT and combination of HNT and PHBV-g-MA on the thermal degradation of PHBV/PBS 80/20 blends can be seen in Fig. 12a and b. There are no significant changes in thermal properties of PHBV/PBS blend with adding 5 wt% of PHBV-g-MA but the addition of HNT to the polymer blends leads to a decreasing thermal stability of the nanocomposites compared to the neat blend. Similarly, PHBV/PBS blend in presence of PHBV-g-MA and HNT also exhibits the same decomposition process as PHBV/PBS/HNT nanocomposites. The influence of clay on the thermal degradation of PHBV/PBS 80/20 blend is clearly shown when comparing experimental and theoretical TGA curves (Fig. 12c). Theoretical TGA curves were calculated according to Eq. (4):

$$M_{blend} = W_{PHBV}M_{PHBV} + W_{PBS}M_{PBS} + W_{HNT}M_{HNT} \quad (4)$$

**Table 4**

Thermal properties of neat PHBV, neat PBS and PHBV/PBS 80/20 binary blends and PHBV/PBS/HNT nanocomposites with and without PHBV-g-MA compatibilization.

Samples	PHBV						PBS						
	$T_c$ (°C)	$\Delta H_c$ (J/g)	$T_m$ (°C)	$\Delta H_m$ (J/g)	$T_g$ (°C)	$X_c$ (%)	$T_c$ (°C)	$\Delta H_c$ (J/g)	$T_{m1}$ (°C)	$T_{m2}$ (°C)	$\Delta H_m$ (J/g)	$T_g$ (°C)	$X_c$ (%)
PHBV/PBS 80/20	113.2 ± 0.6	64.2 ± 0.3	170.5 ± 0.4	61.3 ± 2.6	1.3 ± 2.3	52.5 ± 0.0	48.4 ± 0.3	3.5 ± 0.21	–	111.4 ± 0.2	10.7 ± 0.2	–	26.8 ± 0.0
PHBV/PBS 80/20 + PHBV-g-MA	113.3 ± 1.8	65.5 ± 0.2	168.8 ± 0.3	59.7 ± 0.6	–1.8 ± 1.2	50.8 ± 0.0	45.2 ± 4.8	3.7 ± 1	–	111.0 ± 0.4	11.0 ± 0.4	–	29.0 ± 0.0
PHBV/PBS 80/20 + HNT	111.7 ± 0.1	55.4 ± 0.1	168.4 ± 1.1	50.7 ± 0.5	–0.3 ± 1.3	45.7 ± 0.0	83.2 ± 0.7	5.5 ± 2.1	–	110.8 ± 0.3	11.9 ± 0.8	–	31.2 ± 0.0
PHBV/PBS 80/20 + HNT + PHBV-g-MA	113.7 ± 0.1	63.1 ± 1.3	170.1 ± 0.1	59.0 ± 1.8	2.9 ± 0.8	52.5 ± 0.0	59.2 ± 3.7	3.0 ± 0.1	–	111.2 ± 0.2	8.4 ± 0.3	–	23.4 ± 0.0

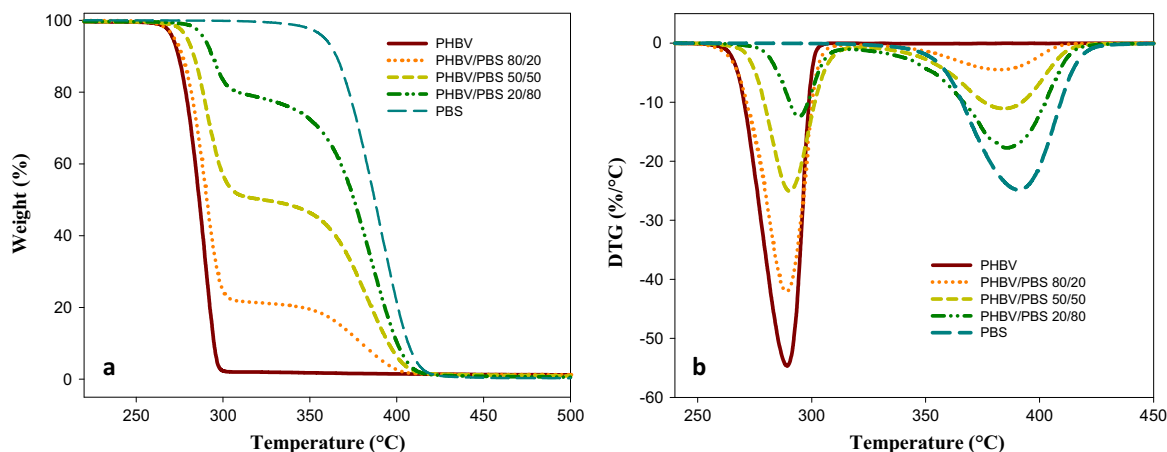


**Fig. 11.** (a) and (b) TGA and DTG curves of neat PHBV, neat PBS and PHBV/PBS blends.

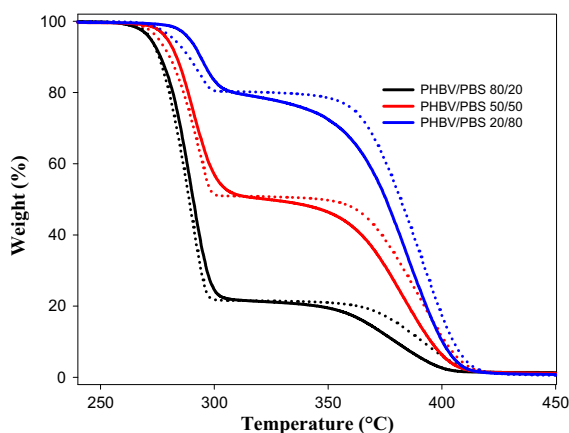


**Fig. 11.** (c) TGA of PHBV/PBS binary blends: continuous lines show the behavior observed experimentally and the dashed lines stands for the theoretical curves according to Eq. (3).

**Table 5**

Decomposition temperatures of PHBV, PBS and PHBV/PBS blends obtained from TGA and DTG.

Samples	$T_{5\%}$ (°C)	$T_{10\%}$ (°C)	$T_{50\%}$ (°C)	$T_{\max}$ (PHBV) (°C)	$T_{\max}$ (PBS) (°C)
PHBV	271	274	286	287	–
PHBV/PBS 80/20	272	276	291	289	382
PHBV/PBS 50/50	279	283	323	290.5	384
PHBV/PBS 20/80	289	294	375	294.5	385.5
PBS	358	365	387	–	390

A noticeable difference between the theoretical and experimental curves is observed. It can be ascribed to the unfavorable effect of HNT on the degradation of PHBV/PBS blend which can be caused by hydrolysis processes affecting polyester matrices through the silanol groups present at the external surface of HNT particles. This result is in accordance with the increasing carbonyl amount in the presence of HNT, as determined by FTIR. Chrissafi and Bikiaris [53] and Bikiaris [54] showed that clay has two antagonist effects on the thermal stability of polymer/clay nanocomposites: (i) a barrier effect that could improve the thermal stability and (ii) a catalyzed degradation effect, caused by silanols through Al Lewis and Brønsted acid sites and, if any by organo-modifiers, that can decrease the thermal stability.

### 3.4. Flammability properties (PCFC)

Table 6a presents the results of PCFC experiments. Fig. 13a shows the heat release rate (HRR) curves of neat polymer and PHBV/PBS binary blends. Two distinct peaks corresponding to PHBV and PBS degradation can be identified, showing that the

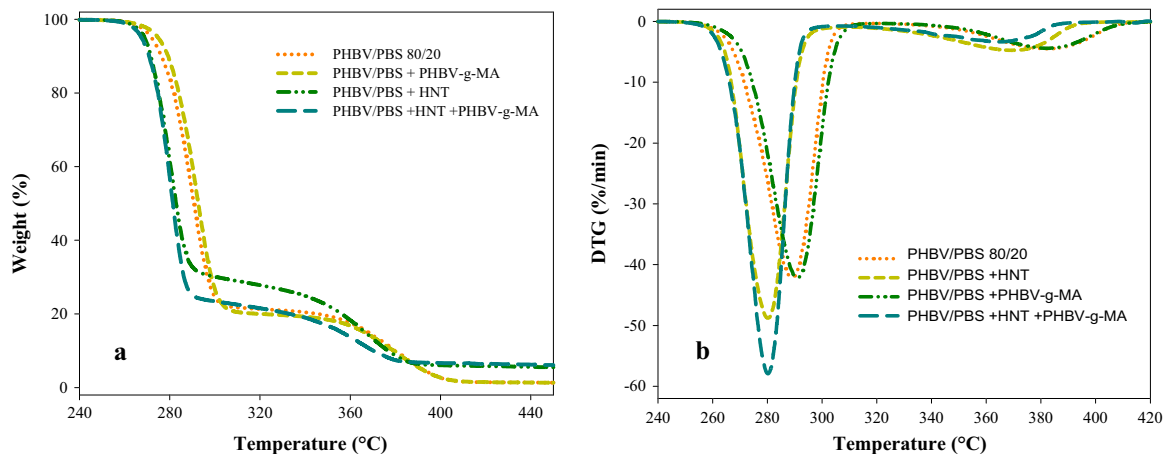


**Fig. 12.** (a and b) TGA and DTG diagrams of PHBV/PBS 80/20 binary blend and PHBV/PBS/HNT nanocomposites with and without PHBV-g-MA compatibilization.

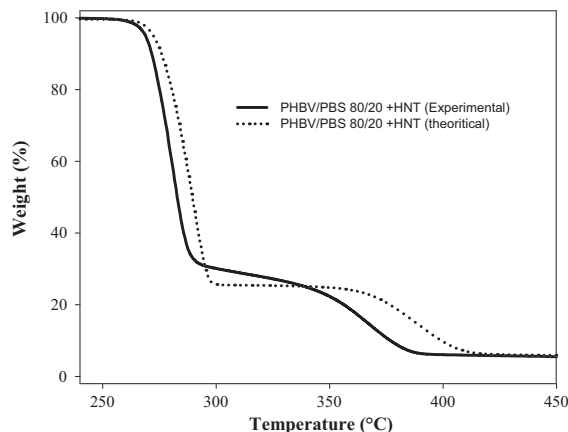


**Fig. 12.** (c) TGA of PHBV/PBS 80/20 + HNT ternary blend: continuous lines show the effect observed experimentally and the dashed line stands for the theoretical curve according to Eq. (4).

**Table 6a**

PCFC data for pure polymers and PHBV/PBS blends.

Samples	$pHRR_{PHBV}$ (W/g)	$pHRR_{PBS}$ (W/g)	$THR_{PHBV}$ (kJ/g)	$THR_{PBS}$ (kJ/g)	$THR_{blend}$ (kJ/g)
PHBV	1027.0 ± 77.2	–	20.6 ± 0.8	–	–
PHBV/PBS 80/20	702.5 ± 37.0	72.1 ± 2.1	16.4 ± 0.1	3.6 ± 0.1	19.8 ± 0.4
PHBV/PBS 50/50	390.0 ± 18.4	176.6 ± 7.0	10.4 ± 0.7	10.1 ± 0.8	20.3 ± 1.2
PHBV/PBS 20/80	298.7 ± 11.0	303.8 ± 11.0	4.7 ± 0.2	15.2 ± 1.3	19.5 ± 0.9
PBS	–	426.1 ± 20.0	–	14.2 ± 0.5	–

**Table 6b**

PCFC parameters of PHBV/PBS 80/20 nanocomposites without and with compatibilization.

Samples	$pHRR_{PHBV}$ (W/g)	$pHRR_{PBS}$ (W/g)	$THR_{PHBV}$ (kJ/g)	$THR_{PBS}$ (kJ/g)	$THR_{blend}$ (kJ/g)
PHBV	1027 ± 77	–	–	–	20.6 ± 0.8
PHBV/PBS 80/20	702.5 ± 37	72.1 ± 2.1	16.4 ± 0.1	3.6 ± 0.1	19.8 ± 0.5
PHBV/PBS 80/20 + PHBV-g-MA	792.0 ± 44	51.6 ± 0.6	14.7 ± 0.5	3.5 ± 0.5	18.4 ± 0.2
PHBV/PBS 80/20 + HNT	584.2 ± 40	86.0 ± 1.5	14.4 ± 0.2	5.0 ± 0.3	19.7 ± 0.3
PHBV/PBS 80/20 + HNT + PHBV-g-MA	738.6 ± 19	77.5 ± 11	16.2 ± 0.6	3.7 ± 0.4	19.6 ± 0.6
PBS	426.1 ± 20	26.15 ± 2	–	–	14.2 ± 0.5

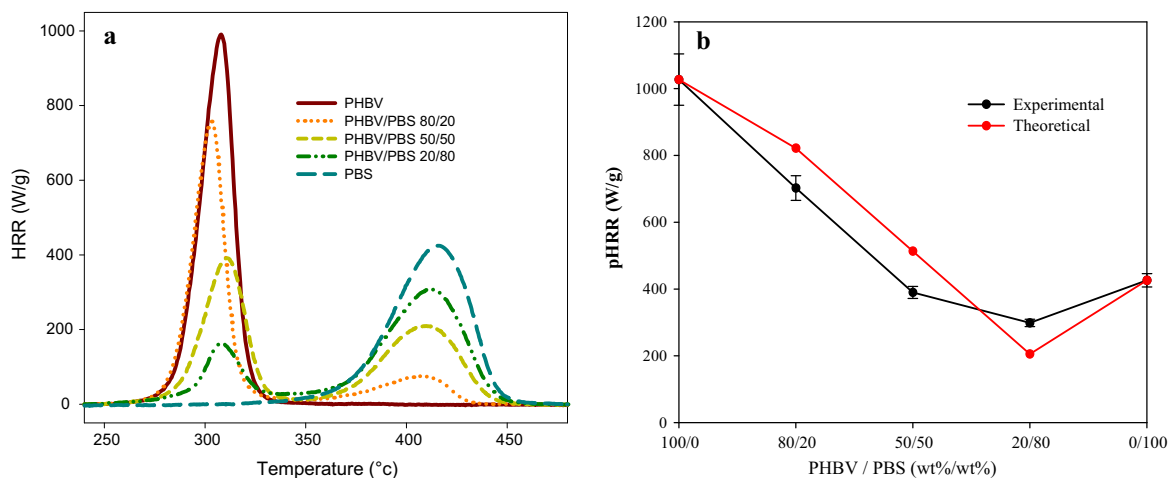


**Fig. 13.** (a) Heat release rate (*HRR*) versus temperature for PHBV, PBS and PHBV/PBS blends; (b) experimental and theoretical values (additive rule of mixture) of *pHRR* of PHBV in blends.

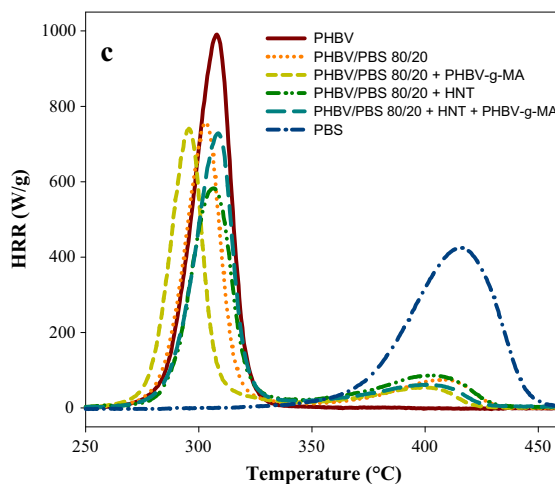


**Fig. 13.** (c) HRR curves of PHBV/PBS 80/20 binary blend and PHBV/PBS/HNT nanocomposites with and without PHBV-g-MA compatibilization.

fire behaviors of both polymers are very different. The peak heat release rate (*pHRR*) of PHBV is far higher than that of PBS. The high *pHRR* of PHBV as compared to others biopolyesters has already been reported in literature [21]. This highlights a greater flammability of PHBV because the chemical environment around ester linkages involves their easier cleavage, and hence plays a role in its thermal stability and released products during thermal degradation. Blending PHBV with PBS allows the *pHRR* to be reduced more strongly than the rule of mixture for the compositions in which the fraction of PHBV is at least 50% (Fig. 13b). The relative deviation to this rule is the highest for the 50/50 blends, showing the interest of the co-continuous morphology toward fire behavior.

The temperatures corresponding to the degradation peaks of each polymer (PHBV at 306 °C, PBS at 414 °C) remain unchanged for the PHBV in the blend (except for the PHBV/PBS 80/20 composition), while it is slightly decreases for PBS with increasing amount of PHBV.

The study of the total heat release values for the blends (*THR*) shows that *THR* does not vary significantly between the different blends and neat PHBV (around 20 kJ/g). *THR* for PBS alone is particularly low (around 14 kJ/g) in comparison with PHBV/PBS blends and neat PHBV. Generally, the decrease of the *THR* associated to each polymer in function of its percentage in the blend follows an additive rule of mixture. Consequently, the influence of blends composition and microstructure appears only visible on *pHRR* and not on *THR* values.

Fig. 13c and Table 6b present the influence of PHBV-g-MA and HNT on the fire retardancy of the 80/20 PHBV/PBS blends. The presence of HNT in the blend leads to a considerable reduction of *pHRR*, whereas the temperature peak is unchanged.

HNT may have modified the decomposition products of the blend since  $THR_{PHBV}$  decreases while  $THR_{PBS}$  increases. FTIR-PCFC coupling should brought information about the combustion mechanisms and decomposition products of the PHBV/PBS/HNT nanocomposites. The incorporation of PHBV-g-MA involves a significant increase of  $pHRR$ , suggesting that the energy release rate of PHBV-g-MA is higher than that of PHBV due to the presence of the maleic anhydride group. Finally, the combination of both HNT and PHBV-g-MA seems to level the influence of each of these components since the PCFC parameters are very close to those of the neat blend.

#### 4. Conclusions

PHBV/PBS immiscible blends were prepared by melt compounding at different weight ratios (80/20, 50/50 and 20/80 w/w). The PHBV/PBS 80/20 blend showed a nodular morphology whereas a co-continuous morphology was observed at 50 wt% of PBS in PHBV. DSC experiments revealed that the addition of PBS limits the crystallization of PHBV and TGA investigations indicated that PBS is much more thermally stable than PHBV. Adding PBS in PHBV induced an enhancement of the overall thermal stability of the resulting blends. Theoretical TGA curves indeed showed that PHBV degrades at higher temperature for all blends. PCFC data clearly show that neat PHBV releases much more energy than neat PBS during combustion. However, the peak of heat released rate of PHBV was decreased by the addition of PBS.

The PHBV/PBS 80/20 blend was selected to investigate the effect of maleic anhydride-grafted PHBV (PHBV-g-MA) compatibilizer and HNTs, on the microstructure and thermal properties of ternary PHBV/PBS/HNT nanocomposites. SEM micrographs and image analysis confirmed that the nodular morphology of PHBV/PBS was refined by adding PHBV-g-MA. The size distribution of PBS nodules was indeed greatly decreased due to the migration of PHBV-g-MA chains to the interfacial area that reduce the interfacial tension between PHBV and PBS. The dispersion of HNTs in the blend also reduced to a lesser extent the size of PBS nodules. However, combining HNTs with PHBV-g-MA limited the emulsifying effect of PHBV-g-MA. Although being not fully elucidated, it is postulated that PHBV-g-MA and HNT interact to form aggregates that could limit the PHBV-g-MA chains diffusion at the PHBV/PBS interface. The DSC and TGA thermograms indicated that the emulsifying effect of PHBV-g-MA had no significant influence on the thermal properties and crystallization of PHBV/PBS blend. In contrast, the incorporation of HNT (or combining HNT with PHBV-g-MA) in the 80/20 blend promoted its thermal degradation. The calculation of theoretical TGA curves indeed showed that HNTs lower the thermal decomposition temperature of the ternary nanocomposite. However, the presence of HNT in the PHBV/PBS blend led to an improvement of their fire reaction, characterized by a significant decrease of the heat release rate of PHBV.

Concluding, this set of results demonstrates the interest of preparing PHBV/PBS blends and the possibility to control their structure and thermal properties by compatibilization with PHBV-g-MA or the addition of HNT nanoparticles. Improved dispersion of PBS nodules can be obtained by both strategies. Moreover, HNT nanoparticles involve more significant changes in the thermal properties. Combining PHBV-g-MA/HNT seems to level these effects, and efforts should be made to better characterize and control the localization of each component within the ternary PHBV/PBS/HNT nanocomposites. To this respect, a control of the processing steps and/or the compatibilization of HNTs could be considered.

#### Acknowledgments

This work was supported by the international program EGIDE through the TASSILI (PHC Hubert Curien) program 13 MDU 891. The authors are grateful to Jean-Jacques Robin, Olinda Gimello, Loïc Dumazert, Jean-Marie Taulemesse, Gaëtan Garreffa for their help in the experimental work.

#### References

- [1] Q. Zhang, Q. Liu, J.E. Mark, I. Noda, A novel biodegradable nanocomposite based on poly (3-hydroxybutyrate-co-3-hydroxyhexanoate) and silylated kaolinite/silica core-shell nanoparticles, *Appl. Clay Sci.* 46 (2009) 51–56.
- [2] H. Schmitt, K. Prashantha, J. Soulestin, M.F. Lacrampe, P. Krawczak, Preparation and properties of novel melt-blended halloysite nanotubes/wheat starch nanocomposites, *Carbohydr. Polym.* 89 (2012) 920–927.
- [3] P. Phukon, J.P. Saikia, B.K. Konwar, Bio-plastic (P-3HB-co-3HV) from *Bacillus circulans* (MTCC 8167) and its biodegradation, *Colloids Surf. B Biointerf.* 92 (2012) 30–34.
- [4] M.R. Nanda, M. Misra, A.K. Mohanty, The effects of process engineering on the performance of PLA and PHBV blends, *Macromol. Mater. Eng.* 296 (2011) 719–728.
- [5] H. Zhao, Z. Cui, X. Wang, L.S. Turng, X. Peng, Processing and characterization of solid and microcellular poly(lactic acid)/polyhydroxybutyrate-valerate (PLA/PHBV) blends and PLA/PHBV/Clay nanocomposites, *Compos. B Eng.* 51 (2013) 79–81.
- [6] M. Avella, E. Martuscelli, M. Raimo, Properties of blends and composites based on poly(3-hydroxy)butyrate (PHB) and poly(3-hydroxybutyrate-hydroxyvalerate) (PHBV) copolymers, *J. Mater. Sci.* 35 (2000) 523–545.
- [7] J. Wang, Z. Wang, J. Li, B. Wang, J. Liu, P. Chen, et al, Chitin nanocrystals grafted with poly(3-hydroxybutyrate-co-3-hydroxyvalerate) and their effects on thermal behavior of PHBV, *Carbohydr. Polym.* 87 (2012) 784–789.
- [8] Q.S. Liu, M.F. Zhu, W.H. Wu, Z.Y. Qin, Reducing the formation of six-membered ring ester during thermal degradation of biodegradable PHBV to enhance its thermal stability, *Polym. Degrad. Stab.* 94 (2009) 18–24.
- [9] Q. Liu, T.-W. Shyr, C.-H. Tung, Z. Liu, G. Shan, M. Zhu, et al, Particular thermal properties of poly(3-hydroxybutyrate-co-3-hydroxyvalerate) oligomers, *J. Polym. Res.* 19 (2011) 9756.
- [10] I. Zembouai, M. Kaci, S. Bruzaud, A. Benhamida, Y.-M. Corre, Y. Grohens, A study of morphological, thermal, rheological and barrier properties of Poly(3-hydroxybutyrate-Co-3-Hydroxyvalerate)/polylactide blends prepared by melt mixing, *Polym. Test* 32 (2013) 842–851.
- [11] M. Nar, G. Staufenberg, B. Yang, L. Robertson, R.H. Patel, V.G. Varanasi, et al, Osteoconductive bio-based meshes based on Poly(hydroxybutyrate-co-hydroxyvalerate) and poly(butylene adipate-co-terephthalate) blends, *Mater. Sci. Eng. C* 38 (2014) 315–324.

- [12] V. Nagarajan, M. Misra, A.K. Mohanty, New engineered biocomposites from poly(3-hydroxybutyrate-co-3-hydroxyvalerate) (PHBV)/poly(butylene adipate-co-terephthalate) (PBAT) blends and switchgrass: fabrication and performance evaluation, *Ind. Crops Prod.* 42 (2013) 461–468.
- [13] J. Tao, C. Song, M. Cao, D. Hu, L. Liu, N. Liu, et al, Thermal properties and degradability of poly(propylene carbonate)/poly( $\beta$ -hydroxybutyrate-co- $\beta$ -hydroxyvalerate) (PPC/PHBV) blends, *Polym. Degrad. Stab.* 94 (2009) 575–583.
- [14] Y.S. Chun, W.N. Kim, Thermal properties of poly(hydroxybutyrate-co-hydroxyvalerate) and poly( $\epsilon$ -caprolactone) blends, *Polymer* 41 (2000) 2305–2308.
- [15] L. Miao, Z. Qiu, W. Yang, T. Ikehara, Fully biodegradable poly(3-hydroxybutyrate-co-hydroxyvalerate)/poly(ethylene succinate) blends: phase behavior, crystallization and mechanical properties, *React. Funct. Polym.* 68 (2008) 446–457.
- [16] Z. Qiu, T. Ikehara, T. Nishi, Miscibility and crystallization behaviour of biodegradable blends of two aliphatic polyesters. Poly(3-hydroxybutyrate-co-hydroxyvalerate) and poly(butylene succinate) blends, *Polymer* 44 (2003) 7519–7527.
- [17] P. Ma, D.G. Hristova-Bogaerds, P.J. Lemstra, Y. Zhang, S. Wang, Toughening of PHBV/PBS and PHB/PBS blends via in situ compatibilization using dicumyl peroxide as a free-radical grafting initiator, *Macromol. Mater. Eng.* 297 (2012) 402–410.
- [18] P. Ma, X. Cai, W. Wang, F. Duan, D. Shi, P.J. Lemstra, Crystallization behavior of partially crosslinked poly( $\beta$ -hydroxyalkanoates)/poly(butylene succinate) blends, *J. Appl. Polym. Sci.* 131 (2014).
- [19] A. Bhatia, R. Gupta, Compatibility of biodegradable poly (lactic acid)(PLA) and poly (butylene succinate)(PBS) blends for packaging application, *Kor.-Aust. Rheol. J.* 19 (2007) 125–131.
- [20] A. Taguet, P. Cassagnau, J.-M. Lopez-Cuesta, Structuration, selective dispersion and compatibilizing effect of (nano)fillers in polymer blends, *Prog. Polym. Sci.* 39 (2014) 1526–1563.
- [21] I. Zembouai, S. Bruzaud, M. Kaci, A. Benhamida, Y.-M. Corre, Y. Grohens, et al, Synergistic effect of compatibilizer and cloisite 30B on the functional properties of poly(3-hydroxybutyrate-co-3-hydroxyvalerate)/polylactide blends, *Polym. Eng. Sci.* 54 (2014) 2239–2251.
- [22] B. Bittmann, R. Bouza, L. Barral, M. Castro-Lopez, S. Dopico-Garcia, Morphology and thermal behavior of poly (3-hydroxybutyrate-co-3-hydroxyvalerate)/poly(butylene adipate-co-terephthalate)/clay nanocomposites, *Polym. Compos.* 36 (2015) 2051–2058.
- [23] J.P. Mofokeng, A.S. Luyt, Morphology and thermal degradation studies of melt-mixed poly(hydroxybutyrate-co-valerate) (PHBV)/poly( $\mu$ -caprolactone) (PCL) biodegradable polymer blend nanocomposites with TiO<sub>2</sub> as filler, *J. Mater. Sci.* 50 (2015) 3812–3824. z.
- [24] M. Murariu, A.-L. Dechief, Y. Paint, S. Peeterbroeck, L. Bonnaud, P. Dubois, Poly(lactide) (PLA)—halloysite nanocomposites: production, morphology and key-properties, *J. Polym. Environ.* 20 (2012) 932–943.
- [25] A. Hao, I. Wong, H. Wu, B. Lisco, B. Ong, A. Salleau, et al, Mechanical, thermal, and flame-retardant performance of polyamide 11-halloysite nanotube nanocomposites, *J. Mater. Sci.* 50 (2015) 157–167.
- [26] H. Han, X. Wang, D. Wu, Mechanical properties, morphology and crystallization kinetic studies of bio-based thermoplastic composites of poly(butylene succinate) with recycled carbon fiber, *J. Chem. Technol. Biotechnol.* 88 (2013) 1200–1211.
- [27] E. Joussein, S. Petit, J. Churchman, B. Theng, D. Righi, B. Delvaux, Halloysite clay minerals – a review, *Clay Miner.* (2005) 40383–40426.
- [28] M. Liu, Z. Jia, D. Jia, C. Zhou, Recent advance in research on halloysite nanotubes-polymer nanocomposite, *Prog. Polym. Sci.* 39 (2014) 1498–1525.
- [29] M. Du, B. Guo, D. Jia, Newly emerging applications of halloysite nanotubes: a review, *Polym. Int.* 59 (2010) 574–582.
- [30] D. Rawtani, Y.K. Agrawal, Multifarious applications of halloysite nanotubes: a review, *Rev. Adv. Mater. Sci.* 30 (2012) 282–295.
- [31] P. Russo, B. Vetrano, D. Acierno, M. Mauro, Thermal and structural characterization of biodegradable blends filled with halloysite nanotubes, *Polym. Compos.* 34 (2012) 1460–1470.
- [32] K. Iggui, N. Le Moigne, M. Kaci, S. Cambe, J.-R. Degorce-Dumas, A. Bergeret, A biodegradation study of poly(3-hydroxybutyrate-co-3-hydroxyvalerate)/organoclay nanocomposites in various environmental conditions, *Polym. Degrad. Stab.* 119 (2015) 77–86.
- [33] Y.S. Salim, A.A.-A. Abdullah, C.S.S.M. Nasri, M.N.M. Ibrahim, Biosynthesis of poly(3-hydroxybutyrate-co-3-hydroxyvalerate) and characterisation of its blend with oil palm empty fruit bunch fibers, *Bioresour. Technol.* 102 (2011) 3626–3628.
- [34] K. Issaadi, A. Habi, Y. Grohens, I. Pillin, Effect of the montmorillonite intercalant and anhydride maleic grafting on polylactic acid structure and properties, *Appl. Clay Sci.* 107 (2015) 62–69.
- [35] C. Chen, S. Peng, B. Fei, Y. Zhuang, L. Dong, Z. Feng, et al, Synthesis and characterization of maleated poly(3-hydroxybutyrate), *J. Appl. Polym. Sci.* 88 (2003) 659–668.
- [36] P.J. Barham, A. Keller, E.L. Otun, P.A. Holmes, Crystallization and morphology of a bacterial thermoplastic: poly-3-hydroxybutyrate, *J. Mater. Sci.* 19 (1984) 2781–2794.
- [37] W. Zhu, X. Wang, X. Chen, K. Xu, Miscibility, crystallization, and mechanical properties of poly(3-hydroxybutyrate-co-4-hydroxybutyrate)/ poly (butylene succinate) blends, *J. Appl. Polym. Sci.* 114 (2009) 3923–3932.
- [38] R.E. Lyon, R.N. Walters, Pyrolysis combustion flow calorimetry, *J. Anal. Appl. Pyrol.* 71 (2004) 27–46.
- [39] P. Ma, D.G. Hristova-Bogaerds, Y. Zhang, P.J. Lemstra, Enhancement in crystallization kinetics of the bacterially synthesized poly( $\beta$ -hydroxybutyrate) by poly(butylene succinate), *Polym. Bull.* 71 (2014) 907–923.
- [40] H.J. Jin, B.Y. Lee, M.N. Kim, J.S. Yoon, Properties and biodegradation of poly(ethylene adipate) and poly(butylene succinate) containing styrene glycol units, *Eur. Polym. J.* 36 (2000) 2693–2698.
- [41] R. Shogren, Starch-poly(hydroxyalkanoate) composites and blends, in: L. Yu (Ed.), *Biodegrad. Polym. Blends Compos. from Renew. Resour.*, John Wiley & Sons, Inc., 2009, pp. 211–226.
- [42] X. Wang, Z. Chen, X. Chen, J. Pan, K. Xu, Miscibility, crystallization kinetics, and mechanical properties of poly(3-hydroxybutyrate-co-3-hydroxyvalerate)(PHBV)/poly(3-hydroxybutyrate-co-4-hydroxybutyrate)(P3/4HB) blends, *J. Appl. Polym. Sci.* 117 (2010) 838–848.
- [43] A. Buzarovska, A. Grozdanov, Crystallization kinetics of poly(hydroxybutyrate-co-hydroxyvalerate) and poly(dicyclohexylitaconate) PHBV/PDCHI blends: thermal properties and hydrolytic degradation, *J. Mater. Sci.* 44 (2009) 1844–1850.
- [44] T. Furukawa, H. Sato, R. Murakami, J. Zhang, Y.X. Duan, I. Noda, et al, Structure, dispersibility, and crystallinity of poly(hydroxybutyrate)/ poly(L-lactic acid) blends studied by FT-IR microspectroscopy and differential scanning calorimetry, *Macromolecules* 38 (2005) 6445–6454.
- [45] S. Singh, A.K. Mohanty, T. Sugie, Y. Takai, H. Hamada, Renewable resource based biocomposites from natural fiber and polyhydroxybutyrate-co-valerate (PHBV) bioplastic, *Compos. A Appl. Sci. Manuf.* 39 (2008) 875–886.
- [46] J. John, J. Tang, Z. Yang, M. Bhattacharya, Synthesis and characterization of anhydride-functional polycaprolactone, *Polym. Sci. A Polym. Chem.* 35 (1996) 1139–1148.
- [47] P. Maiti, C.A. Batt, E.P. Giannelis, New biodegradable polyhydroxybutyrate/layered silicate nanocomposites, *Biomacromolecules* 8 (2007) 3393–3400.
- [48] P. Bordes, E. Pollet, L. Avérous, Nano-biocomposites: biodegradable polyester/nanoclay systems, *Prog. Polym. Sci.* 34 (2009) 125–155.
- [49] X. Wang, J. Zhou, L. Li, Multiple melting behavior of poly(butylene succinate), *Eur. Polym. J.* 43 (2007) 3163–3170.
- [50] M. Yasuniwa, S. Tsubakihara, T. Satou, K. Iura, Multiple melting behavior of poly(butylene succinate). II. Thermal analysis of isothermal crystallization and melting process, *J. Polym. Sci. Part B Polym. Phys.* 43 (2005) 2039–2047.
- [51] Z. Qiu, T. Ikehara, T. Nishi, Poly(hydroxybutyrate)/poly(butylene succinate) blends: miscibility and nonisothermal crystallization, *Polymer* 44 (2003) 2503–2508.
- [52] R.T. Tol, V.B.F. Mathot, G. Groeninckx, Confined crystallization phenomena in immiscible polymer blends with dispersed micro- and nanometer sized PA6 droplets, part 1: uncompatibilized PS/PA6, (PPE/PS)/PA6 and PPE/PA6 blends, *Polymer* 46 (2005) 369–382.
- [53] K. Chrissafis, D. Bikiaris, Can nanoparticles really enhance thermal stability of polymers? Part I: an overview on thermal decomposition of addition polymers, *Thermochim. Acta* 523 (2011) 1–24.
- [54] D. Bikiaris, Can nanoparticles really enhance thermal stability of polymers? Part II: an overview on thermal decomposition of polycondensation polymers, *Thermochim. Acta* 523 (2011) 25–45.